From nappe stacking to out-of-sequence postcollisional deformations: Cretaceous to Quaternary exhumation history of the SE Carpathians assessed by low-temperature thermochronology

S. Merten,[1,2] L. Matenco,[1,3] J. P. T. Foeken,[4,5] F. M. Stuart,[4] and P. A. M. Andriessen[1,2]

Received 8 June 2009; revised 13 November 2009; accepted 13 January 2010; published 26 June 2010.

[1] Apatite fission track (AFT) and (U-Th)/He (AHe) thermochronology have been combined to constrain the exhumation history of the SE Carpathians. Cooling ages generally decrease from Cretaceous for the internal basement nappes (AFT ages), to Miocene–Quaternary (AFT and AHe, respectively) for the external sedimentary wedge. The AFT and AHe data show a Paleogene age cluster, which confirms a suspected but never demonstrated tectonic event. The new data furthermore suggest that the SE Carpathians have been affected by a middle Miocene exhumation phase related to continental collision, which occurred at rates of ~0.8 mm/yr, similar to the one previously inferred for the East Carpathians. The SE Carpathian tectonic evolution, however, is overprinted by two younger exhumation events in the Pliocene–Pleistocene. The first exhumation phase (latest Miocene–early Pliocene) occurred at high exhumation rates (~1.7 mm/yr) and is interpreted as a tectonic event and/or associated with a sea level drop in the Paratethys basins during the Messinian low stand. The youngest recorded tectonic phase suggests rapid Pleistocene exhumation (~1.6 mm/yr) and is interpreted to represent crustal-scale shortening different in mechanics from collisional processes. The data suggest that the SE Carpathians did not develop as a typical double-vergent orogenic wedge; instead, exhumation was related to a foreland-vergent sequence of nappe stacking during collision and was subsequently followed by a large out-of-sequence shortening event truncating the already locked collisional boundary.

Citation: Merten, S., L. Matenco, J. P. T. Foeken, F. M. Stuart, and P. A. M. Andriessen (2010), From nappe stacking to out-of-sequence postcollisional deformations: Cretaceous to Quaternary exhumation history of the SE Carpathians assessed by low-temperature thermochronology, *Tectonics*, *29*, TC3013, doi:10.1029/2009TC002550.

1. Introduction

[2] The relationship between the construction/destruction of an orogen and the transport/infill in the adjacent sedimentary basin results from a complex interplay between tectonic and surface processes. The resulting mass redistribution drives uplift and erosion in the orogen and subsidence and sedimentation in the foreland basin. The typical geometry of a foredeep as shown by modeling studies assumes a sedimentary wedge formed by flexure due to thrust loading, which migrates in time toward the foreland due to subduction [e.g., *Beaumont*, 1981]. When the nonthinned crustal part of the lower plate arrives at the subduction zone (i.e., during collision) the convergence gradually stops, the foreland basin undergoes a regressive stage of complete basin fill and is exhumed due to postcollisional rebound. This typical model is often at odds with observations derived from seismic studies, which demonstrate significant subsidence of the foreland basin and the external part of the orogenic wedge in the postcollisional stage and/or renewed out-of-sequence contractional episodes [e.g., *Bertotti et al.*, 2006]. This has been explained by the postcollisional evolution of the remnant slab, which can impact the geometry of foredeep wedges by vertical movements associated with processes such as detachment or delamination [e.g., *Sacks and Secor*, 1990; *Wortel and Spakman*, 2000]. However, some of the abnormal foredeep geometries cannot be explained only by the evolution of the slab, and can be alternatively explained by other processes, such as lithospheric folding in the case of the Carpathians [e.g., *Bertotti et al.*, 2003].

[3] Models of subduction generally predict that mountain chains will develop in double-vergent orogenic wedges during collision and that denudation amplifies the hinterland exhumation along retroshears [e.g., *Beaumont et al.*, 1994]. In such orogens, exhumational steady state, i.e., the balance between topography, erosion and temperature distribution, assumes that reset thermochronological age zones will be nested adjacent to the retrodeformation front [e.g., *Willett and Brandon*, 2002]. However, many orogens do not appear to indicate obvious enhanced contractional exhumation in the orogenic core during collision. This is observed in Mediterranean-type orogens, such as the Apennines,

[1]Netherlands Research Centre for Integrated Solid Earth Science, Amsterdam, Netherlands.
[2]Department of Isotope Geochemistry, Faculty of Earth and Life Sciences, VU University, Amsterdam, Netherlands.
[3]Department of Tectonics, Faculty of Earth and Life Sciences, VU University, Amsterdam, Netherlands.
[4]Isotope Geosciences Unit, Scottish Universities Environmental Research Centre, East Kilbride, UK.
[5]Now at Department of Isotope Geochemistry, Faculty of Earth and Life Sciences, VU University, Amsterdam, Netherlands.

0278-7407/10/2009TC002550

Dinarides, Calabria and the Betics [*Jolivet and Faccenna*, 2000]. Most of these chains develop back-arc basins during convergence [*Faccenna et al.*, 2004] and can be defined as subduction-dominated orogens, i.e., where the subduction velocity is higher than the convergence velocity [*Royden and Burchfiel*, 1989].

[4] The SE Carpathians (Figure 1) are an example of such an orogenic system that lacks enhanced exhumation in the orogenic core. It forms a highly arcuate mountain belt associated with a large back-arc basin (i.e., Pannonian Basin, Figure 1). Within the Carpathian system, the collisional evolution of the SE Carpathians and adjacent Focşani foredeep basin shows some striking features. Following the cessation of early to middle Miocene nappe stacking, a Pliocene to Quaternary exhumation phase took place synchronous with abnormally high subsidence in its foredeep basin [e.g., *Tărăpoancă et al.*, 2003]. The foredeep reveals continuous latest Miocene–Pliocene subsidence, subsequently followed by early Quaternary inversion and tilting of strata [*Matenco et al.*, 2007]. However, in the adjacent orogenic nappe pile the timing of this renewed contraction and associated uplift appears to have started earlier, at around 5–6 Ma. This is indicated by thermochronological studies [*Sanders et al.*, 1999] and a petrological change in the sediment sources of the foredeep deposits [*Panaiotu et al.*, 2007]. The force driving this two-stage postcollisional evolution (subsidence followed by renewed contraction) is not well understood, but is generally attributed to processes taking place in the already subducted slab (such as delamination) (see *Knapp et al.* [2005] for a review), or to intraplate deformation [e.g., *Cloetingh et al.*, 2004]. In this context, understanding the postcollisional exhumation history provides key near-surface constraints on the overall lithospheric evolution.

[5] Deformation episodes in the Carpathians are traditionally dated using posttectonic covers [e.g., *Săndulescu*, 1988] (Figure 2). Quantitative thermochronological constraints on the exhumation history related to these deformations are available for the South Carpathians [*Fügenschuh and Schmid*, 2005, and references therein] or for isolated parts in the East Carpathians [e.g., *Gröger et al.*, 2008] (Figure 1). No quantitative constraints on the pre-Miocene evolution of the SE Carpathians are available. These are, however, critical for unraveling the unusual collisional geometry of the SE Carpathians. This is because a large part of the rotation and translation of the Tisza-Dacia upper plate unit around the Moesian lower plate (Figure 1) took place during the Paleogene [e.g., *Fügenschuh and Schmid*, 2005]. This movement of the upper plate would imply shortening in the East and SE Carpathians, which is not defined so far.

[6] A large number of uncertainties exist concerning the mechanisms, timing and rates of exhumation of the final evolutional stages of low-topography orogens such as the Carpathians. This is largely due to the fact that exhumation is in the order of a few kilometers and thus outside the resolution of most thermochronometers. However, with the application of apatite fission track (AFT) and apatite (U-Th)/He (AHe) thermochronology with low closure temperatures of 120–80°C and 85–40°C, respectively, the location, timing and rates of Cretaceous–Quaternary exhumation in the SE Carpathians can be assessed.

2. Evolution of the East and SE Carpathians and Kinematic Constraints

[7] The Carpathians are an arcuate fold-and-thrust belt, which resulted from N–S convergence between a puzzle of continental domains situated between the main Apulian/Adriatic and Eurasian plates [e.g., *Csontos and Vörös*, 2004, and references therein] (Figure 1b). In the Romanian Carpathians, the Alpine kinematics can be briefly summarized as the evolution of three continental domains which have closed two oceans. At the interior, the East Vardar Ocean (or Transylvanides), part of the Neotethys, was situated between the Tisza and Dacia continental blocks (Figure 1b) [see *Schmid et al.*, 2008]. It opened during Triassic–Jurassic times, gradually closed and underwent subduction/obduction during Late Jurassic–Cretaceous times followed by continental collision in the late Early Cretaceous [e.g., *Schmid et al.*, 2008, and references therein]. At the exterior, the Ceahlău-Severin Ocean, part of the Alpine Tethys, opened between the Dacia block and the European/Moesian foreland during Late Jurassic–Early Cretaceous times (Figure 1b) and was subsequently closed by subduction recorded in Cretaceous to Miocene contractional episodes [e.g., *Ştefănescu*, 1976; *Schmid et al.*, 2008].

2.1. Cretaceous Convergence of Ceahlău-Severin

[8] In the East and SE Carpathians, Cretaceous convergence of the Ceahlău-Severin Ocean resulted in intra-Albian and intra-Senonian tectonic events affecting both the upper continental block (Dacia) and the sediments deposited in the Ceahlău-Severin oceanic domain [*Săndulescu*, 1988] (Figure 1). The former is composed of the so-called Bucovinian nappe stack (Figure 1a), which contains metamorphic series of Late Precambrian to Cambrian age [e.g., *Kräutner and Bindea*, 2002] and an Upper Carboniferous to Mesozoic sedimentary cover. Lower Cretaceous sediments grade into a prelower Albian wildflysch. This sequence is found underneath the overriding ophiolite-bearing Transylvanian nappes derived from the obduction of the East Vardar Ocean. Tectonic contacts among the three Bucovinian nappes are sealed

Figure 1. (a) Tectono-structural map of the SE Carpathians (modified after *Vasiliev* [2006], *Săndulescu* [1984], *Visarion et al.* [1988], and *Matenco et al.* [2003]). Contours in the Focşani Basin indicate depth of Quaternary deposits [*Matenco et al.*, 2007]. Solid black line marks the cross sections of Figures 5a and 7a. Dashed black ellipse indicates Vrancea seismogenic zone. (b) Tectonic map of the Eastern Alps-Carpathians-Dinarides-Balkans region (simplified after *Schmid et al.* [2008]) with solid box indicating the location of the SE Carpathians (Figure 1a). White lines indicate the outlines of the Pannonian and Transylvania basins. Dashed black line indicates the border of Romania. (c) Topography of the Carpathians-Dinarides-Pannonian system in Europe with solid box indicating the location of Figure 1b.

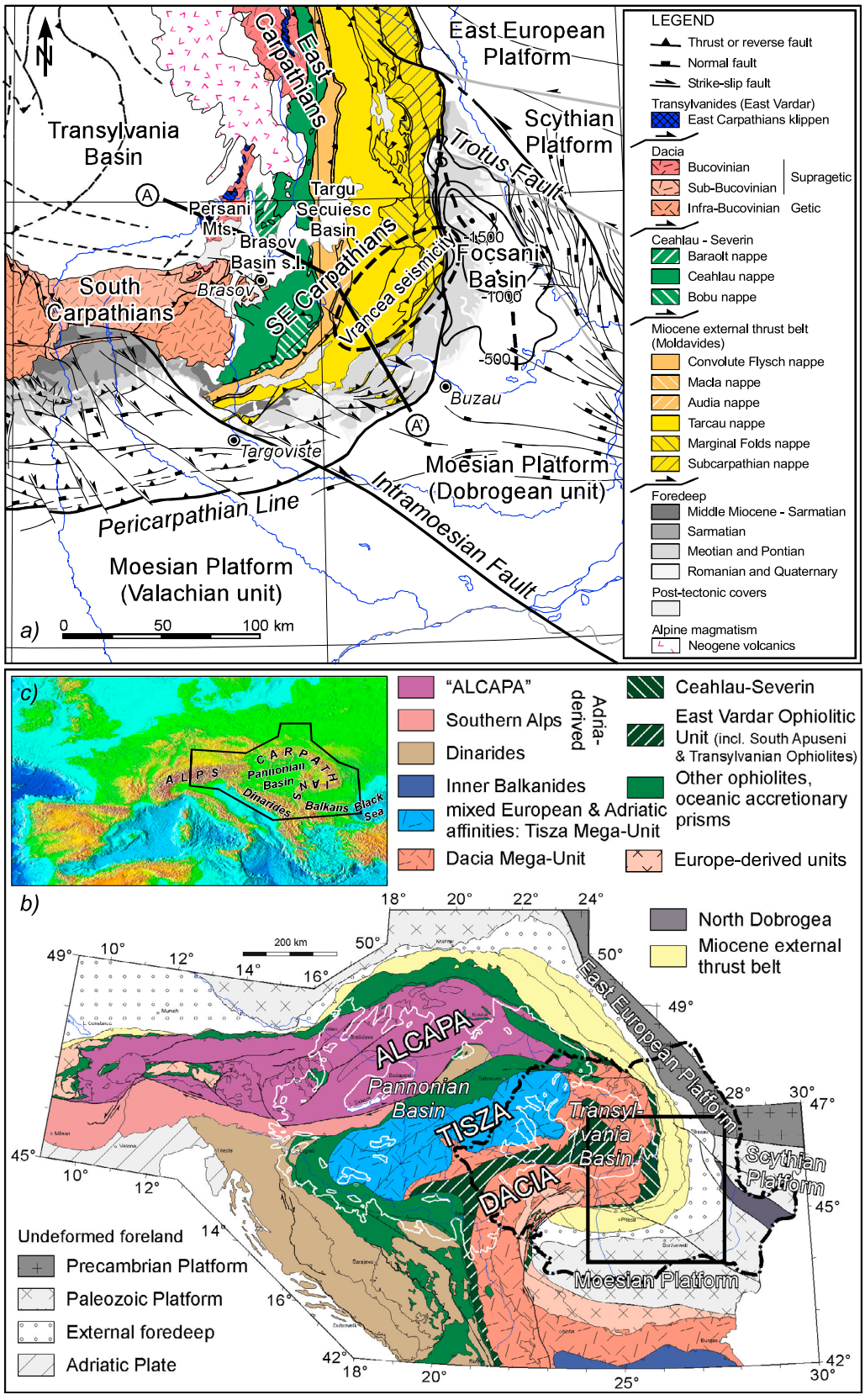
a)
East Carpathians
East European Platform
Transylvania Basin
Scythian Platform
Trotus Fault
Targu Secuiesc Basin
Persani Mts.
Brasov Basin s.l.
Brasov
South Carpathians
SE Carpathians
Vrancea seismicity
Focsani Basin
-1500
-1000
-500
Buzau
Targoviste
Moesian Platform (Dobrogean unit)
Intramoesian Fault
Pericarpathian Line
Moesian Platform (Valachian unit)
0 50 100 km
LEGEND
Thrust or reverse fault
Normal fault
Strike-slip fault
Transylvanides (East Vardar)
East Carpathians klippen
Dacia
Bucovinian
Sub-Bucovinian
Infra-Bucovinian
Supragetic
Getic
Ceahlau - Severin
Baraolt nappe
Ceahlau nappe
Bobu nappe
Miocene external thrust belt (Moldavides)
Convolute Flysch nappe
Macla nappe
Audia nappe
Tarcau nappe
Marginal Folds nappe
Subcarpathian nappe
Foredeep
Middle Miocene - Sarmatian
Sarmatian
Meotian and Pontian
Romanian and Quaternary
Post-tectonic covers
Alpine magmatism
Neogene volcanics
c)
CARPATHIANS
ALPS
Pannonian Basin
Dinarides
Balkans
Black Sea
"ALCAPA"
Southern Alps
Dinarides
Inner Balkanides
mixed European & Adriatic affinities: Tisza Mega-Unit
Dacia Mega-Unit
Adria-derived
Ceahlau-Severin
East Vardar Ophiolitic Unit (incl. South Apuseni & Transylvanian Ophiolites)
Other ophiolites, oceanic accretionary prisms
Europe-derived units
b)
200 km
North Dobrogea
Miocene external thrust belt
East European Platform
ALCAPA
Pannonian Basin
TISZA
Transylvania Basin
DACIA
Scythian Platform
Moesian Platform
Undeformed foreland
Precambrian Platform
Paleozoic Platform
External foredeep
Adriatic Plate

Figure 1

by an upper Albian to lower Cenomanian posttectonic cover [e.g., *Ştefănescu*, 1976; *Kräutner*, 1980].

[9] The ophiolite-bearing Ceahlău unit (and its South Carpathian equivalent, the Severin nappe) forms a wedge accreted onto the overlying continental Dacian units (Bucovinian-Getic nappes, Figure 1a) during the intraAlbian tectonic event [e.g., *Săndulescu*, 1988]. During the same intraAlbian event, the most internal thrust sheet of the Ceahlău unit (Baraolt nappe, Figure 1a) was deformed, as indicated by the upper Albian–Cenomanian posttectonic cover (Figure 2) [e.g., *Ştefănescu*, 1976]. The intraSenonian event led to the thrusting of the main body of the Ceahlău unit over the depositional area of the future Miocene external thrust belt (Figure 1), as demonstrated by the late Campanian–Maastrichtian posttectonic cover (Figure 2) [e.g., *Săndulescu*, 1988; *Melinte and Jipa*, 2005].

2.2. Miocene Contraction of the External East and SE Carpathians

[10] The subsequent tectonic evolution of the Miocene external thrust belt [*Săndulescu*, 1988] was driven by subduction retreat of a slab derived from the Ceahlău-Severin Ocean into the so-called "Carpathian embayment." This concave-shaped embayment follows the present day curved configuration of the Carpathians and was situated in a more eastward position relative to the Ceahlău-Severin paleogeographic domain (Figure 1) [*Balla*, 1987; *Ustaszewski et al.*, 2008]. Closure of the embayment culminated with the late Miocene continental collision of the Tisza-Dacia block with the European/Moesian foreland [*Săndulescu*, 1988; *Morley*, 1996].

[11] The Miocene external thrust belt of the East and SE Carpathians comprises Cretaceous to Miocene clastic sediments (mostly turbidites, Figure 2) presently nappe stacked over the European foreland (senso-largo, including the distal parts of the Moesian and Scythian platforms, Figure 1). Thrusting of the Miocene external thrust belt took place gradually toward the foreland as dated by posttectonic covers (Figure 2) and can be subdivided into three different substages [*Ştefănescu*, 1976; *Săndulescu*, 1988]. The Convolute Flysch, Macla and Audia nappes (Figure 1a) were stacked during early Burdigalian times (18–20 Ma). The Tarcău and Marginal Folds nappes (Figure 1a) were internally stacked and thrust onto their foreland during the middle Miocene (latest Burdigalian–Badenian, 17–15.5 Ma). At the beginning of the late Miocene (~11 Ma), the most frontal Subcarpathian nappe (Figure 1a) was thrust over the present-day "undeformed" foreland [e.g., *Matenco and Bertotti*, 2000]. The basal sole thrust at the front of the SE Carpathians (Pericarpathian Line, Figure 1a) is covered by uppermost Miocene–Quaternary sediments, thus indicating that the main thrusting episode terminated during the late Miocene (middle Sarmatian, ~11 Ma, Figure 2) [e.g., *Dumitrescu and Săndulescu*, 1968]. The general interpretation is that collision was locked from this moment onward and generalized exhumation of the mountain belt occurred, except for the SE Carpathians [e.g., *Cloetingh et al.*, 2004].

3. Postcollisional Deformation in the SE Carpathians

[12] After the late Miocene termination of thrusting in the Carpathians, postcollisional deformation affected the area of the SE Carpathians only (Figure 1a). Here, post–11 Ma to as young as Quaternary sediments of the foredeep (Figure 1a, the Focşani Basin) are deformed [e.g., *Hippolyte and Săndulescu*, 1996; *Tărăpoancă et al.*, 2003; *Leever et al.*, 2006, and references therein]. Synkinematic thickness variations have been recorded from the uppermost Pliocene onward and lower Quaternary coarse deposits have been subsequently tilted (~5–10° eastward dip) and uplifted to present-day elevations of up to 1 km [e.g., *Leever et al.*, 2006] (Figure 2). In the SW areas (Figure 1a, between Buzău and Târgovişte) open folds and thrusts have triggered the remobilization of earlier salt diapirs [e.g., *Ştefănescu et al.*, 2000]. Structures linked with this deformation phase are oblique and out-of-sequence relative to the structural grain of the Miocene external thrust belt [see *Hippolyte and Săndulescu*, 1996]. In contrast to the ~2 Ma onset of deformation indicated by the inversion of foredeep strata as young as lower Quaternary, sandstone petrography data record a change in the source area around 5 Ma, from a volcanic arc province derived from the hinterland volcanoclastic edifices [see also *Seghedi et al.*, 2004] (Figure 1a), to a recycled orogen province [*Panaiotu et al.*, 2007] (Figure 2).

[13] The postcollisional deformation structures in the SE Carpathians have been attributed to a large number of potential geodynamic processes, in an effort to explain the high-velocity mantle anomaly and strong intermediate-mantle seismicity presently observed beneath the Vrancea area (Figure 1a) [e.g., *Oncescu and Bonjer*, 1997; *Martin et al.*, 2006]. Popular geodynamic models such as various types of slab detachment, slab delamination, thermal reequilibration, large-scale lithospheric/crustal folding or gravitational instability of the mantle lithosphere have been proposed (see discussion from *Matenco et al.* [2007]). Whichever geodynamic model is preferred, they all invoke an initial Miocene slab retreat/rollback [see *Royden and Burchfiel*, 1989] as the principal driving force for the formation of the Miocene nappe pile.

4. Low-Temperature Thermochronology of the SE Carpathians

[14] To reconstruct the tectonic evolution of SE Carpathians, vertical movements were traced along a ~150 km long NW–SE trending iso-elevation transect (average elevation 580 ± 130 m) crossing the SE Carpathian orogen from

Figure 2. General time correlation table, lithological columns and tectonogram for the SE Carpathians [after *Săndulescu et al.*, 1981; *Necea et al.*, 2005; *Matenco and Bertotti*, 2000]. Time correlation table between Tethys and Paratethys and absolute ages are taken from *Haq et al.* [1987], *Rögl* [1996], and *Gradstein et al.* [2004]. Italic ages in the Sarmatian–Romanian interval are from the magnetostratigraphic results of *Vasiliev et al.* [2004]. Note the change in time scaling at 23 Ma.

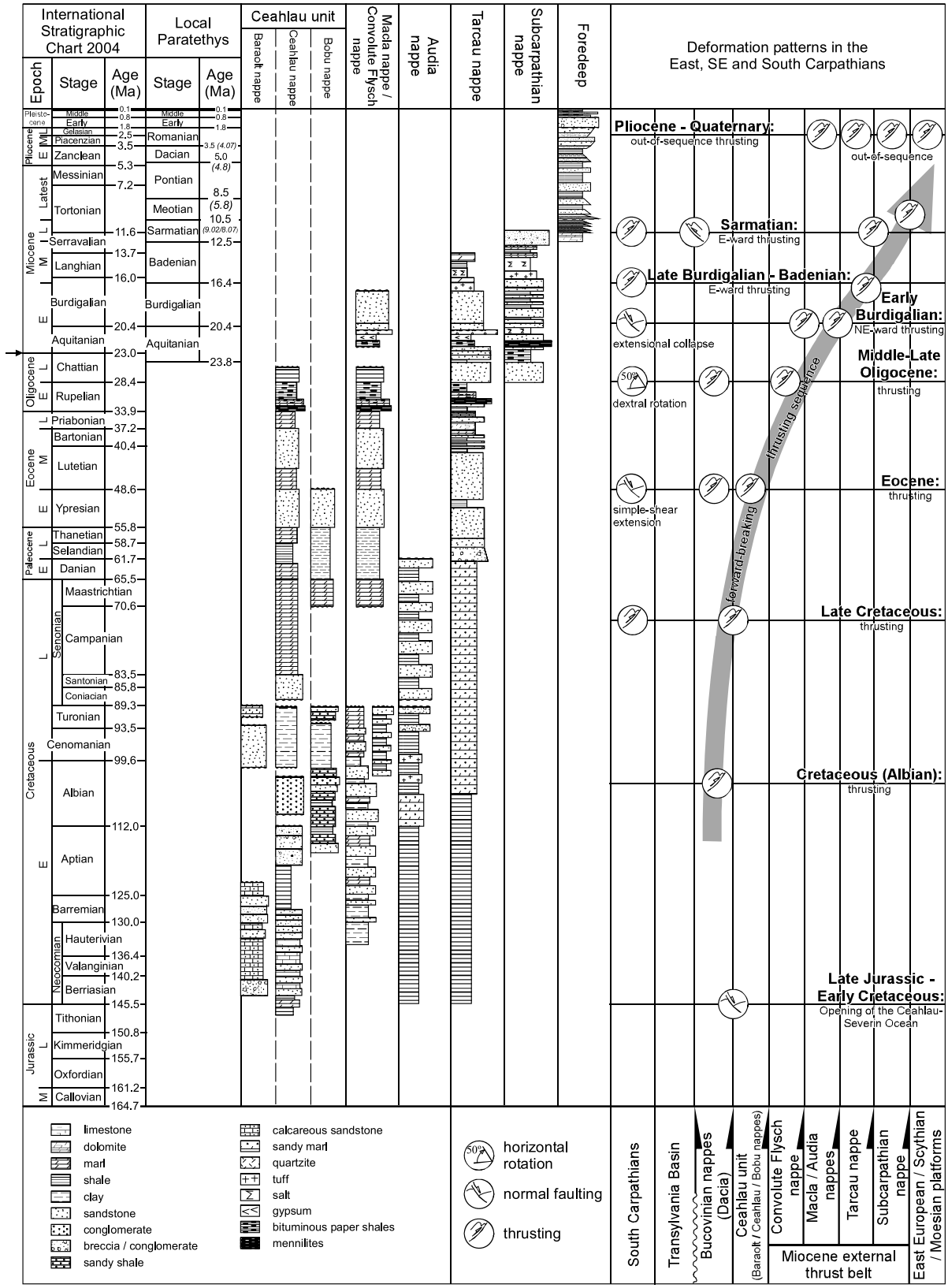
International Stratigraphic Chart 2004
Local Paratethys
Ceahlau unit
Baraolt nappe
Ceahlau nappe
Bobu nappe
Macla nappe / Convolute Flysch nappe
Audia nappe
Tarcau nappe
Subcarpathian nappe
Foredeep
Deformation patterns in the East, SE and South Carpathians
Pliocene - Quaternary:
out-of-sequence thrusting
out-of-sequence
Sarmatian:
E-ward thrusting
Late Burdigalian - Badenian:
E-ward thrusting
Early Burdigalian:
NE-ward thrusting
extensional collapse
Middle-Late Oligocene:
thrusting
dextral rotation
thrusting sequence
Eocene:
thrusting
simple-shear extension
forward-breaking
Late Cretaceous:
thrusting
Cretaceous (Albian):
thrusting
Late Jurassic - Early Cretaceous:
Opening of the Ceahlau-Severin Ocean
limestone
dolomite
marl
shale
clay
sandstone
conglomerate
breccia / conglomerate
sandy shale
calcareous sandstone
sandy marl
quartzite
tuff
salt
gypsum
bituminous paper shales
mennilites
horizontal rotation
normal faulting
thrusting
South Carpathians
Transylvania Basin
Bucovinian nappes (Dacia)
Ceahlau unit (Baraolt / Ceahlau / Bobu nappes)
Convolute Flysch nappe
Macla / Audia nappes
Tarcau nappe
Subcarpathian nappe
Miocene external thrust belt
East European / Scythian / Moesian platforms

Figure 2

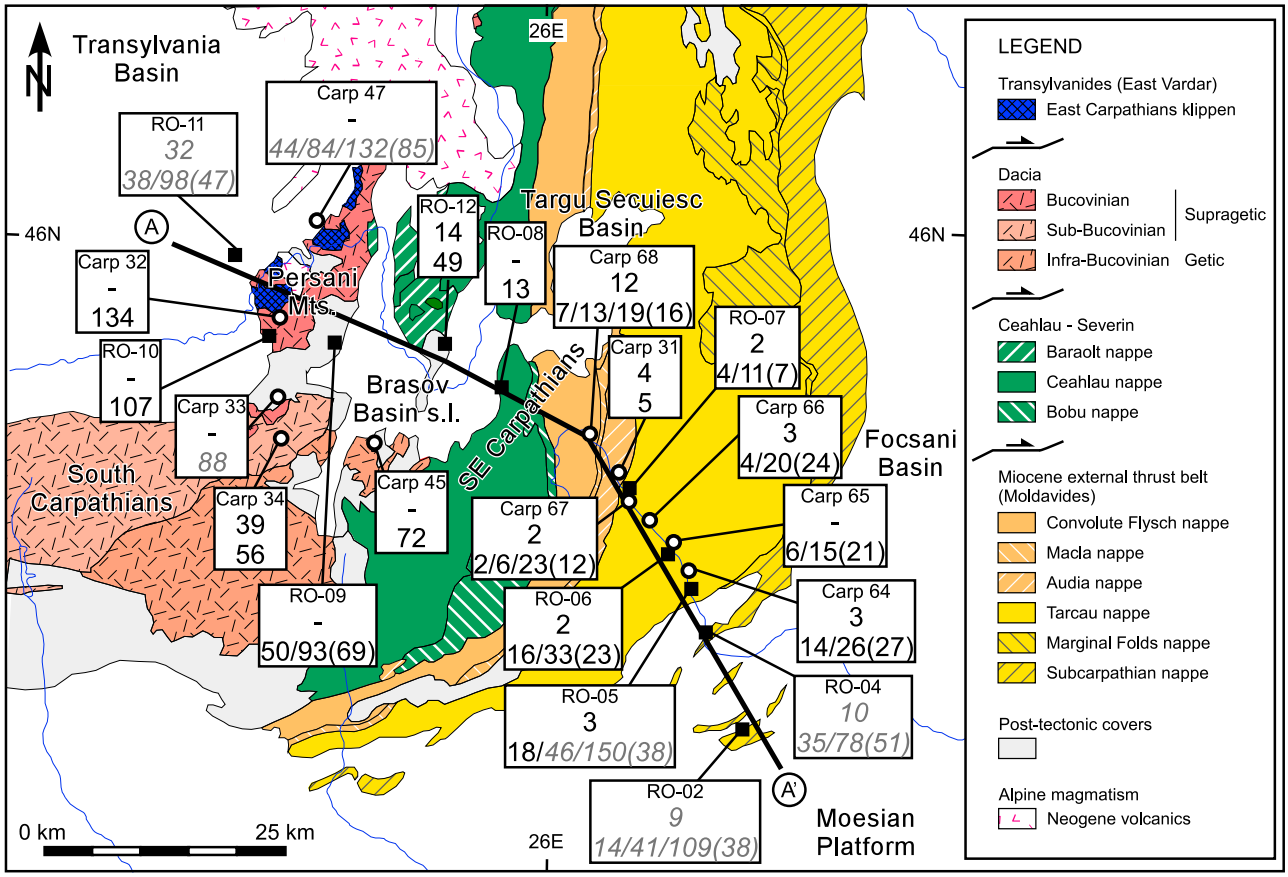

Figure 3. Simplified map of the SE Carpathians [after *Săndulescu*, 1984; *Visarion et al.*, 1988; *Matenco et al.*, 2003] with solid black line marking the cross sections of Figures 5a and 7a. Black squares and open circles mark sample locations of this study and the study of *Sanders et al.* [1999], respectively. Numbers in boxes from top to bottom represent sample code, AHe age and AFT age, respectively. Depicted AHe ages are the error weighted averages of the α-corrected single grain ages (see Tables 3 and 4). For homogeneous samples AFT central ages are shown. For heterogeneous samples all AFT age populations and the central ages (in brackets) are depicted. Ages in grey italics represent nonreset ages (i.e., provenance ages).

the Transylvania hinterland basin to the Focşani foredeep basin (Figure 3). In total 16 clastic sediment samples were analyzed for AFT and AHe thermochronology (Table 1). Of the 16 samples, six were already measured for AFT [*Sanders et al.*, 1999] but reassessed by AHe (Table 1); 10 new samples were collected.

4.1. Apatite Fission Track Thermochronology (AFT)

[15] Apatites were separated from whole rock using standard mineral separation procedures. The 90–200 μm grain size range was handpicked to take out the nonapatites, as regular mineral separation procedures did not yield pure apatite selections. Two mounts were prepared for each sample; one for age determinations (on 21 to 80 grains) and one for confined track length measurements. Fission track ages are central ages [*Galbraith and Laslett*, 1993] and were calculated with TRACKKEY version 4.2.g [*Dunkl*, 2000]. The Chi-square (χ^2) test [*Galbraith*, 1981; *Brandon*, 1992] was used to assess the homogeneity of the age population for each sample (Table 2). Only two of the ten samples returned P(χ^2) values of >5% and dispersions <30% (RO-10 and RO-12), indicating homogeneous age populations (Table 2). One sample with a P(χ^2) value >1% and a dispersion <30% (RO-08) was also considered as homogeneous. The other seven samples have P(χ^2) values <1% and dispersions >30%, indicating mixed age distributions (Table 2). The program BINOMFIT (developed by M. Brandon and summarized by *Ehlers et al.* [2005]) was used to decompose ages for mixed age distributions in the heterogeneous samples.

[16] The samples yielded low spontaneous fission track densities for track length measurements, thus tracks-in-track (TINT) fission track densities were enhanced prior to etching, using ^{252}Cf-derived fission fragment tracks [*Donelick and Miller*, 1991]. For each sample 31 to 136 horizontal confined tracks were measured (Table 2). Confined track lengths are normalized for track angle using the c axis projection model of *Donelick et al.* [1999] to increase the consistency of the measurements and to compensate for Cf-irradiation and observer bias [e.g., *Barbarand et al.*, 2003; *Ketcham*, 2005b; *Ketcham et al.*, 2007]. Etch pit diameters (D_{par}) were measured on both age and track length mounts [*Donelick*, 1993; *Ketcham et al.*, 1999]. All statistical uncertainties on ages and

Table 1. Overview Sample Properties and Thermochronology Results[a]

Sample Code	Elevation (m)	Tectonic Unit	Petrography	Stratigraphic Age (Ma)	AFT Central Age (Ma)	AFT Central ±1σ	Data Type	Intra-Albian Age (Ma)	Intra-Albian ±1σ	Intra-Senonian Age (Ma)	Intra-Senonian ±1σ	Paleogene Age (Ma)	Paleogene ±1σ	Early Miocene Age (Ma)	Early Miocene ±1σ	Middle Miocene Age (Ma)	Middle Miocene ±1σ	Late Miocene Age (Ma)	Late Miocene ±1σ	Plio-Quaternary Age (Ma)	Plio-Quaternary ±1σ
RO-11	470	5) Transylvanian hinterland	Sandstone	16.0–12.5 (Badenian)	*46.9*	*5.9*	AFT[b]	*98*	*32*			*38*	*8*								
							AHe[d]					*32*	*2*								
RO-10	520	1) Bucovinian nappe	Schist	-	107.3	13.8	AFT[c]	107	14												
Carp 32[e]	700	1) Bucovinian nappe	Schist	-	134	18	AFT[c]	134	18												
Carp 47[e]	700	5) Transylvanian hinterland	Sandstone	23.8–5.3 (Miocene)	*85*	*6*	AFT[f]	*132*	*13*	*84*	*4*	*44*	*4*								
Carp 33[e]	700	5) Transylvanian hinterland	Sandstone	33.9–23.0 (Oligocene)	*88*	*8*	AFT[c]			*88*	*8*										
Carp 34[e]	700	1) Sub-Bucovinian nappe	Schist	-	56	4	AFT[c]					56	4								
							AHe[d]					39	6								
RO-09	700	3) Cretaceous posttectonic cover	Conglomerate	98.9–93.5 (Albian-Cenomanian)	68.6	7.6	AFT[b]			93	23	50	13								
Carp 45[e]	800	3) Cretaceous posttectonic cover	Sandstone	98.9–93.5 (Albian-Cenomanian)	72	5	AFT[c]			72	5										
RO-12	580	2) Baraolt nappe	Conglomerate	125.0–112.0 (Aptian)	48.5	5.5	AFT[c]					49	6								
							AHe[d]									14	1				
RO-08	550	2) Ceahlau nappe	Conglomerate	130.0–112.0 (Barremian-Aptian)	12.7	2.0	AFT[c]									13	2				
Carp 68[e]	680	4) Convolute flysch nappe	Sandstone	112.0–99.6 (Albian)	16	4	AFT[f]							19	5	13	7	7.0	3.0		
							AHe[d]									12	2				
Carp 31[e]	700	4) Audia nappe	Sandstone	89.3–65.5 (Senonian)	5	1	AFT[c]													5.0	1.0
							AHe[d]													4.3	0.2
RO-07	650	4) Tarcau nappe	Sandstone	65.5–40.4 (Paleocene-Lutetian)	7.2	1.1	AFT[b]									11	3			3.8	1.6
							AHe[d]													2.2	0.1
Carp 67[e]	630	4) Tarcau nappe	Sandstone	55.8–33.9 (Eocene)	12	3	AFT[f]							23	5			6.0	1.0	2.0	1.0
							AHe[d]													2.0	0.1
Carp 66[e]	620	4) Tarcau nappe	Sandstone	33.9–23.0 (Oligocene)	24	6	AFT[f]							20	1					4.0	1.0
							AHe[d]													3.2	0.5
Carp 65[e]	500	4) Tarcau nappe	Sandstone	55.8–33.9 (Eocene)	21	6	AFT[f]									15	2	6.0	2.0		
RO-06	470	4) Tarcau nappe	Sandstone	65.5–40.4 (Paleocene-Lutetian)	23.1	2.6	AFT[b]					33	7			16	4				
							AHe[d]													1.9	0.1
Carp 64[e]	430	4) Tarcau nappe	Sandstone	65.5–23.0 (Paleogene)	27	7	AFT[f]							26	3	14	2				
							AHe[d]													3.4	0.4
RO-05	395	4) Tarcau nappe	Sandstone	37.2–23.0 (Priabonian-Chattian)	*38.3*	*5.9*	AFT[b]	*150*	*62*			*46*	*11*	18	5						
							AHe[d]													3.3	0.4
RO-04	370	6) Foredeep	Sandstone	10.5–8.5 (Meotian)	*51.1*	*6.2*	AFT[b]			*78*	*21*	*35*	*8*								
							AHe[d]											*9.9*	*0.8*		
RO-02	350	6) Foredeep	Sandstone	11.5–10.5 (Top Sarmatian)	*37.8*	*4.9*	AFT[b]	*109*	*24*			*41*	*9*			*14*	*4*				
							AHe[d]											*9.2*	*0.6*		

[a]Ages in italics represent nonreset ages.
[b]AFT age populations calculated with BINOMFIT [*Brandon*, 2002], this study.
[c]AFT central age, this study and *Sanders et al.* [1999].
[d]AHe error weighted average age, this study.
[e]Samples analyzed for AFT by *Sanders et al.* [1999]; 6 of these samples were reanalyzed by AHe thermochronology in this study.
[f]AFT age components, *Sanders et al.* [1999].

Table 2. Apatite Fission Track Analytical Data[a]

Sample Code[b]	N	ρ_s ($\times 10^6 cm^{-2}$)	N_s	ρ_i ($\times 10^6 cm^{-2}$)	N_i	$P(\chi^2)$ (%)	Age ± 1σ (Ma)	Disp. (%)	U (ppm)	Pop. 1 (Ma)	95% Cl. (−/+)	Ab. (%)	Pop. 2 (Ma)	95% Cl (−/+)	Ab. (%)	Pop. 3 (Ma)	95% Cl (−/+)	Ab. (%)	MTL ± 1σ (μm)	SD_L (μm)	N_L	D_{par} (μm)	SD_{Dpar} (μm)
RO-02	80	0.372	1742	1.403	6570	0.0	37.8 ± 4.9	68	17.8	13.9	3.4/4.5	34	40.7	8.1/10.1	51	108.5	21.1/26.1	14	13.77 ± 0.12	1.14	86	1.3	0.3
RO-04	51	0.593	1056	2.177	3879	0.0	51.1 ± 6.2	40	24.3	35.2	7.0/8.7	62	78.2	17.9/23.2	38				13.25 ± 0.14	1.15	68	1.2	0.3
RO-05	37	0.399	534	2.042	2732	0.0	38.3 ± 5.9	63	24.3	18.3	4.2/5.5	45	45.7	9.9/12.6	45	149.7	49.8/74.3	10	13.54 ± 0.10	1.13	120	1.6	0.4
RO-06	76	0.199	1056	1.455	7719	0.0	23.1 ± 2.6	36	16.6	16.4	3.4/4.2	57	32.5	6.5/8.1	43				12.35 ± 0.10	1.12	136	1.2	0.3
RO-07	40	0.055	205	1.321	4895	0.0	7.2 ± 1.1	48	15.1	3.8	1.3/1.9	47	10.5	2.7/3.6	53				11.62 ± 0.33	1.85	31	1.2	0.2
RO-08	21	0.092	96	1.242	1291	1.3	12.7 ± 2.0	27	13.4										11.73 ± 0.29	1.94	46	1.1	0.2
RO-09	78	0.426	1681	1.026	4045	0.0	68.6 ± 7.6	31	12.4	50.3	11.6/15.1	52	92.5	20.3/25.9	48				14.04 ± 0.11	0.86	61	1.1	0.1
RO-10	32	0.265	354	0.418	559	59.5	107.3 ± 13.8	18	4.9										12.71 ± 0.21	1.43	48	1.0	0.1
RO-11	43	0.586	913	2.218	3458	0.0	46.9 ± 5.9	41	24.3	37.6	7.3/9.0	83	97.9	26.7/36.6	17				14.21 ± 0.13	0.98	60	1.2	0.4
RO-12	55	0.305	829	1.023	2786	7.2	48.5 ± 5.5	20	11.3										12.93 ± 0.12	1.17	89	1.1	0.2

[a]Grains were mounted in epoxy resin and subsequently grinded and polished to reveal the apatites surface. Apatites for age determination were etched for 40 seconds in 1.6 M nitric acid at 21°C to reveal spontaneous tracks [*Murrell*, 2003]. Samples were dated by external detector method (EDM) with muscovite detectors [*Gleadow and Duddy*, 1981] and irradiated at the low-flux reactor of the ECN in Petten, the Netherlands. Two CN5 dosimeter glasses of known uranium content with external mica detectors [*Hurford and Green*, 1982; 1983; *Wagner and van den Haute*, 1992] were included to determine the neutron flux during irradiation. After irradiation, the external mica detectors of samples and dosimeter glasses were etched in 48% hydrofluoric acid at 21°C for 12 and 25 minutes, respectively. TINT fission track densities in length mounts were enhanced prior to etching using ^{252}Cf-derived fission fragment tracks [*Donelick and Miller*, 1991]. Subsequently mounts were etched in 1.6 M nitric acid for 40 seconds at 21°C. Tracks in apatites and micadetectors were counted with an Olympus BX51 optical microscope with 500× magnification using dry objective. Lengths of horizontal confined tracks and etch pits (D_{pars}) were measured with a magnification of 1000×. Positioning of the grain mount and mica mirror image was driven by the AUTOSCAN™ Systems Pty Ltd computerized microscope stage. AFT ages were determined using the Zeta calibration approach [*Hurford and Green*, 1983], $\zeta = 323 \pm 32$ for apatite and dosimeter glass CN-5 (for S. Merten).

[b]Abbreviations are as follows: N is number of dated apatite crystals; ρ_s (ρ_i) are spontaneous (induced) track densities; N_s (N_i) are the number of spontaneous (induced) tracks counted; dosimeter track density (ρ_d) for this set of samples is 1.032×10^6 tracks/cm^2 with 15,177 tracks counted on the dosimeter (N_d); $P(\chi^2)$ is probability obtaining Chi-square (χ^2) for n degrees of freedom (where n is number of crystals minus 1); age is central age [*Galbraith and Laslett*, 1993]; ±1σ is 1σ standard error; Disp. is dispersion in single grain ages; U is U-content in parts per million; Pop. 1–3 are age populations calculated with BINOMFIT [*Brandon*, 2002] for samples that do not pass $P(\chi^2)$ at 5% and with dispersions >30%; 95% Cl is the 95% confidence level for the population; Ab. (%) is the abundance of the age component in the total single grain age distribution of a sample. MTL ± 1σ is c axis projected mean track length ± 1σ standard error; SD_L is standard deviation of track length distribution; N_L is number of measured horizontal confined tracks; D_{par} is average etch pit diameter with SD_{Dpar} its standard deviation.

mean track lengths (MTLs) are quoted at the $\pm 1\sigma$ level (Table 2).

4.2. Apatite (U-Th)/He Thermochronology (AHe)

[17] Inclusion-free apatite grains were carefully hand-picked in alcohol under polarized light. Selected grains were photographed and dimensions were measured for α-ejection correction [*Farley*, 2002]. Single grain replicates (2 to 6) have been analyzed for all samples.

[18] Ten single grain samples (Table 3) were analyzed at SUERC. Apatites were packed in 99.9% pure Pt tubes, and helium was extracted following procedures of *Foeken et al.* [2006]. Because of the sometimes low ^{4}He yield in the samples (Table 3), system blanks were routinely monitored throughout the day (minimum of 2 per day, total blanks measured n = 24). ^{4}He blanks yielded $3.3 \times 10^{-12} \pm 2.8 \times 10^{-13}$ ccSTP (n = 5) for RO-samples marked "L" and $1.8 \times 10^{-12} \pm 3.1 \times 10^{-13}$ ccSTP (n = 19) for the remaining samples. Laser heated empty Pt tubes yielded indistinguishable ^{4}He blanks of $2.5 \times 10^{-12} \pm 5.0 \times 10^{-13}$ ccSTP (n = 3). Thirty analyses required blank corrections of <10%; 14 analyses are between 10 to 50% (Table 3). Reextracts were routinely run for each sample, and were all within system background levels.

[19] Helium measurements for six samples were performed at VU University Amsterdam (VUA, Table 4). Helium was extracted by loading apatites into Inconell cups and heated by an external furnace, following procedures of *Foeken et al.* [2003]. System background blanks were assessed by heating empty Inconell cups and yielded daily averages ranging from $2.4 \times 10^{-12} \pm 3.4 \times 10^{-13}$ to $9.3 \times 10^{-12} \pm 1.7 \times 10^{-12}$ ccSTP (n = 2 to 5). Blanks contributed up to 35% and blank corrections have been applied (Table 4). Reextracts were routinely run for each sample, and were all within system background levels.

[20] Following Helium extraction, apatites were prepared for U and Th analyses following procedures of *Balestrieri et al.* [2005] (SUERC samples) and *Foeken et al.* [2003] (VUA samples). Instrument, full procedure and Pt blanks were measured to assess U and Th background levels. Pt tube blanks for laser heated samples yielded 0.9 ± 0.1 pg and 6.0 ± 0.6 pg (^{238}U and ^{232}Th, respectively, n = 2). Of the 44 analyses, six required U blank corrections between 10 to 28% (Table 3). The three analyses of RO-10 required corrections between 69 to 100% and have not been taken into account for further interpretation because U-quantities were below detection limits of the mass spectrometer (Table 3). For Th, 22 out of 44 laser heated analyses required blank corrections of 10 to 36% (Table 3). Furnace heated samples yielded full procedure blanks of 1.4 ± 0.8 pg and 1.8 ± 1.0 pg (U and Th, respectively, n = 4). Five out of 17 analyses required U blank corrections of 10 to 26%, for one analysis the U-quantity was below detection limit, and three Th analyses required corrections between 10 and 25% (Table 4).

[21] Reported 1σ uncertainties on all ages are propagated from analytical uncertainties on U, Th and He determinations, blank corrections, and uncertainties on grain size measurements for α-correction. For each sample the error weighted average of single grain ages has been calculated, which has subsequently been used for further interpretation. Single grain ages for samples RO-09 and Carp 45 were very disperse and thus these samples have not been taken into account for further interpretation.

[22] Fragments of VU Durango fluorapatite (60–180 μm, 1 to 3 fragments) were analyzed both by laser and furnace. Laser heated Durango ages are 32.8 ± 0.6 Ma (n = 4), which is in excellent agreement with previously reported ages [e.g., *Foeken et al.*, 2006]. Furnace heated Durango ages are slightly older at 35.7 ± 0.4 Ma (n = 5).

4.3. Thermal Modeling

[23] Time–temperature histories were modeled using the HeFTy v 1.3c program *Ketcham* [2005a], using both AFT age and length data and AHe data. Samples with nonreset AFT ages and/or multiple age populations were modeled using the AHe data only. The annealing model of *Ketcham et al.* [1999] was used for the AFT data, which requires the use of the etching procedure as outlined by *Carlson et al.* [1999]. *Carlson et al.* [1999] show that the default initial track length (l_0) systematically correlates with certain measurable parameters including D_{par} ($l_0 = 15.63 + 0.283 \times D_{par}$). Although the VU etching procedure differs from the one by *Carlson et al.* [1999], the annealing model of *Ketcham et al.* [1999] was preferred because it allows correcting for c axis projection and Cf irradiation. The effect of the different etching methods was calibrated by *Murrell* [2003] and *Murrell et al.* [2009], who showed that the average ratio for $D_{par}^{VU}/D_{par}^{Carlson}$ is 1.255 (where D_{par}^{VU} is the etch pit diameter obtained with the VU etching method and $D_{par}^{Carlson}$ is the etch pit diameter obtained with the *Carlson et al.* [1999] etching method). For D_{par} values of 1.0 to 1.6 μm (Table 2) the difference would produce a l_0 of 0.072 to 0.115 μm greater than the "real" value. *Carlson et al.* [1999] stated that 0.5 μm variation in l_0 leads to a difference (overestimation) of 10–15°C in predicted temperature of a time-temperature path. Using the annealing model of *Ketcham et al.* [1999] on our data set would imply an overestimation of 1.4–3.5°C, which is considered negligible in this study and falls within the errors of the modeling process. For the AHe data, the *Farley* [2000] Durango He-diffusion model was used. Whereas more recent diffusion models [e.g., *Shuster et al.*, 2006] have become available, the *Farley* [2000] diffusion model is justified for these samples as they are low in U and Th concentrations [suggesting that alpha-radiation is of minor importance, e.g., *Shuster et al.*, 2006], are not zoned and have been rapidly cooled. The model precision was set to "best fit" to produce the corrected age using the α-ejection correction model of *Farley et al.* [1996]. The present-day surface temperature was set to 10 ± 5°C. Input model constraints are geological constraints (e.g., stratigraphic unconformities and well constrained tectonic phases).

5. Thermochronology Results

[24] Both AFT and AHe reset ages generally decrease along section from the internal Bucovinian basement nappes in the WNW to the Miocene external thin-skinned nappes in the SSE (Figure 3). Total or partial reset AFT ages range from

Table 3. (U-Th)/He Analytical Data Laser Heated Samples[a]

Sample Code	^{4}He[b] (ccSTP)	^{4}He Blank Correction	^{238}U[b] (ng)	^{238}U Blank Correction	^{232}Th[b] (ng)	^{232}Th Blank Correction	Th/U	Uncorrected Age[c] (Ma)	F_T[c]	Corrected Age[c] (Ma)	Error ($\pm1\sigma$)
RO-02											
p1-S[d]	1.66E-11	10%	0.016	5%	0.055	10%	3.6	4.7	0.64	7.4	0.6
p2-S	2.83E-11	6%	0.022	4%	0.081	7%	3.8	5.7	0.64	8.9	1.3
p3-S	2.39E-11	7%	0.017	5%	0.069	8%	4.2	5.9	0.63	9.4	1.6
p1-L	4.84E-11	7%	0.044	2%	0.095	6%	2.2	6.0	0.67	9.0	0.9
p2-L	3.60E-11	9%	0.024	4%	0.094	6%	4.0	6.4	0.68	9.5	2.5
p3-L	9.50E-11	3%	0.069	1%	0.169	3%	2.5	7.2	0.67	10.7	2.0
Average										9.1	1.1
Error weighted average										9.2	0.6
RO-04											
p1-S[d]	9.17E-11	2%	0.032	3%	0.032	16%	1.0	19.2	0.65	29.7	2.2
p2-S	3.36E-12	36%	0.002	28%	0.010	36%	4.6	5.7	0.60	9.6	0.8
p3-S	1.60E-10	1%	0.137	1%	0.098	6%	0.7	8.2	0.59	13.9	2.9
Average										11.7	3.0
Error weighted average										9.9	0.8
RO-05											
p1-S	2.08E-11	8%	0.054	2%	0.082	7%	1.6	2.3	0.62	3.7	0.7
p2-S	9.43E-12	16%	0.022	4%	0.049	11%	2.3	2.3	0.60	3.8	0.9
p3-S	6.79E-12	21%	0.017	5%	0.076	7%	4.7	1.6	0.57	2.8	0.5
Average										3.5	0.6
Error weighted average										3.3	0.4
RO-06											
p1-S	1.91E-11	9%	0.081	1%	0.150	4%	1.9	1.3	0.65	2.1	0.3
p2-S	1.84E-12	50%	0.007	11%	0.026	19%	3.6	1.1	0.67	1.7	0.3
p3-S	1.15E-11	14%	0.065	1%	0.089	6%	1.4	1.1	0.61	1.8	0.3
p1-L[d]	6.57E-12	34%	0.008	10%	0.023	20%	2.9	3.9	0.72	5.4	0.5
p2-L[d]	1.12E-10	3%	0.307	0%	0.490	1%	1.6	2.2	0.71	3.1	0.4
p3-L	7.57E-11	4%	0.377	0%	0.295	2%	0.8	1.4	0.74	1.9	0.3
Average										1.9	0.2
Error weighted average										1.9	0.1
RO-07											
p1-S	3.44E-11	5%	0.130	1%	0.160	4%	1.3	1.7	0.62	2.7	0.4
p2-S	5.81E-12	24%	0.013	7%	0.133	4%	10.7	1.1	0.61	1.8	0.2
p3-S	3.30E-11	5%	0.107	1%	0.216	3%	2.1	1.7	0.61	2.8	0.5
p1-L	3.81E-11	8%	0.089	1%	0.342	2%	4.0	1.8	0.68	2.7	0.5
p2-L	5.22E-11	6%	0.105	1%	0.538	1%	5.2	1.8	0.68	2.7	0.4
p3-L	2.69E-11	11%	0.071	1%	0.306	2%	4.5	1.5	0.70	2.2	0.3
Average										2.5	0.4
Error weighted average										2.2	0.1
RO-09											
p1-S[d]	3.35E-10	1%	0.040	2%	0.016	28%	0.4	63.5	0.60	105.6	6.3
p2-S[d]	9.44E-11	2%	0.020	4%	0.014	31%	0.7	33.3	0.62	53.7	5.8
p3-S[d]	6.70E-10	0%	0.051	2%	0.035	15%	0.7	92.6	0.62	149.0	24.3
p1-L[d]	1.31E-11	21%	0.006	13%	0.013	31%	2.2	11.4	0.70	16.3	1.2
p2-L[d]	1.42E-11	20%	0.007	11%	0.016	27%	2.3	10.5	0.62	17.0	3.7
p3-L[d]	4.60E-10	1%	0.051	2%	0.014	30%	0.3	69.3	0.66	105.8	13.4
Average										-	-
Error weighted average										-	-
RO-10											
p1-S[d]	2.38E-11	7%	B.D.	84%	0.014	30%	-	55.9	0.62	90.4	155.5
p2-S[d]	3.22E-11	5%	B.D.	69%	0.011	35%	-	85.7	0.58	146.5	22.5
p3-S[d]	2.73E-11	6%	B.D.	100%	0.015	28%	-	61.4	0.62	99.1	11.1
Average										-	-
Error weighted average										-	-

Table 3. (continued)

Sample Code	^{4}He[b] (ccSTP)	^{4}He Blank Correction	^{238}U[b] (ng)	^{238}U Blank Correction	^{232}Th[b] (ng)	^{232}Th Blank Correction	Th/U	Uncorrected Age[c] (Ma)	F_T[c]	Corrected Age[c] (Ma)	Error ($\pm1\sigma$)
RO-11											
p1-S	1.96E-10	1%	0.048	2%	0.097	6%	2.1	22.5	0.58	38.7	5.3
p2-S	2.14E-10	1%	0.095	1%	0.017	26%	0.2	17.7	0.62	28.7	3.1
p1-L	2.77E-10	1%	0.062	1%	0.198	3%	3.3	20.9	0.65	32.3	6.7
p2-L[d]	7.32E-10	0%	0.077	1%	0.221	3%	2.9	46.3	0.80	57.7	5.8
p3-L	4.63E-10	1%	0.092	1%	0.268	2%	3.0	24.5	0.63	38.5	8.6
Average										34.6	4.9
Error weighted average										32.0	2.4
RO-12											
p1-S	1.05E-11	15%	0.003	21%	0.040	13%	11.9	6.7	0.57	11.8	2.4
p2-S	2.07E-11	8%	0.014	6%	0.028	18%	2.0	8.1	0.59	13.9	0.8
p1-L	3.07E-11	6%	0.016	5%	0.039	13%	2.5	10.1	0.69	14.8	2.5
Average										13.5	1.5
Error weighted average										13.8	0.8
Carp31											
p1	1.81E-11	9%	0.036	2%	0.033	15%	0.9	3.4	0.76	4.5	0.4
p2	5.33E-12	29%	0.009	9%	0.017	26%	1.9	3.2	0.63	5.1	0.4
p3	1.62E-11	10%	0.051	2%	0.023	20%	0.5	2.4	0.68	3.5	0.4
Average										4.4	0.8
Error weighted average										4.3	0.2
VU Durango											
D11	8.90E-10	0.4%	0.044	2%	0.773	0.8%	18.0	32.3			
D13	1.43E-09	0.1%	0.063	1%	1.216	0.5%	19.7	33.5			
D1	1.13E-09	0.2%	0.042	2%	1.023	0.6%	25.1	32.7			
D2	2.33E-09	0.1%	0.097	1%	2.078	0.3%	22.0	32.6			
Average							21.2	32.8			
Standard deviation							3.1	0.6			

[a]SUERC-measurements following procedures of *Foeken et al.* [2006]. ^{4}He concentrations were calculated by peak height comparison against a calibrated ^{4}He standard, with a reproducibility of 1.4% (1σ, n = 46) for the duration of this set of experiments (July–August 2006). Following He-extraction, apatites were prepared for U and Th measurements following procedures of *Balestrieri et al.* [2005] and spiked with a ^{229}Th/^{233}U spike stock solution.
[b]Blank corrected values; see text for explanation. B.D., below detection limit.
[c]F_T is fraction of alphas retained [*Farley et al.*, 1996]; "corrected ages" are corrected for this effect.
[d]Not taken into account for average and error weighted average.

134 ± 18 to 56 ± 4 Ma (Bucovinian basement) to 2 ± 1 Ma (Miocene external thrust belt, Figures 3, 4 and 5 and Table 1). AHe ages are younger at 39 ± 6 Ma (Bucovinian basement) to 1.9 ± 0.1 Ma (Miocene external thrust belt, Figures 3, 4 and 5 and Table 1). Mean c axis projected track lengths range from 11.62 ± 0.33 to 14.21 ± 0.13 μm (Table 2). Average D_{par} values are between 1.0 ± 0.1 and 1.6 ± 0.4 μm (Table 2) and a fluorine-apatite composition is inferred. No clear correlation could be obtained between D_{par} values versus AFT ages and track lengths. Similarly, *Sanders* [1998] concluded that the statistical age components of the SE Carpathians did not directly correlate with the apatite compositional groups based on etch pit diameter or microprobe analysis. This can be explained by the fact that statistical mixture models analyze the final result of all factors influencing the spread in grain age populations, including not only chemical factors but also provenance ages. Thus for these samples, the obtained AFT age populations are due to provenance and not to composition.

5.1. Thermochronological Ages Versus Depositional Age

[25] In general AFT ages have high dispersions, typically >30% (Table 2 and Figure 4). Only samples with pre-Albian depositional ages (Figure 4a and Tables 1 and 2) yield homogeneous AFT ages that are totally reset, ranging from 134 ± 18 Ma (Early Cretaceous) to 13 ± 2 Ma (middle Miocene). These samples have AHe ages from 39 ± 6 Ma (middle Eocene) to 14 ± 1 Ma (middle Miocene, Figure 4a and Tables 1, 3 and 4). All other samples, i.e., clastic sediments deposited after intraAlbian emplacement of the Bucovinian nappes, returned P(χ^2) values of <5% and dispersions >30% (Figure 4a and Tables 1 and 2). These samples have mixed AFT age populations ranging from 150 ± 62 Ma (Late Jurassic) to 2 ± 1 Ma (Pliocene–Quaternary) (Figure 4 and Tables 1 and 2) that can be explained by heterogeneous annealing of apatites from a variety of sources [*Brandon et al.*, 1998]. The high dispersions indicate reworking of sediments. Upper Cretaceous to upper Eocene sediments have reset AFT age populations ranging from 93 ± 23 Ma to 2 ± 1 Ma. Post-Eocene sediments yield both reset and non-reset AFT age populations ranging from 150 ± 62 Ma to 14 ± 4 Ma (Figure 4 and Table 1), suggesting that this group of samples has not been buried to >110°C since deposition. AHe ages for post-Albian samples are reset and cluster around 12 ± 2 Ma (middle Miocene) and 4.3 ± 0.2 to 1.9 ± 0.1 Ma (Pliocene–Quaternary) (Figure 4 and Tables 1, 3 and 4). Three samples yield nonreset AHe ages of 32 ± 2 Ma

Table 4. (U-Th)He Analytical Data for Furnace Heated Samples[a]

Sample Code	^{4}He[b] (ccSTP)	^{4}He Blank Correction	^{238}U[b] (ng)	^{238}U Blank Correction	^{232}Th[b] (ng)	^{232}Th Blank Correction	Th/U	Uncorrected age[c] (Ma)	F_T[c]	Corrected Age[c] (Ma)	Error ($\pm1\sigma$)
Carp 34											
p1	2.63E-10	3%	0.075	2%	0.005	25%	0.1	28.2	0.73	38.9	6.9
p2	2.67E-10	3%	0.076	2%	0.012	13%	0.2	27.9	0.69	40.4	11.8
Average										39.6	1.1
Error weighted average										39.3	6.0
Carp 45											
p1[d]	5.99E-11	11%	0.033	4%	0.033	5%	1.0	12.1	0.73	16.6	4.6
p3[d]	1.36E-11	35%	B.D.	130%	0.016	10%	-	31.0	0.64	48.4	29.7
p4[d]	3.89E-11	17%	0.005	21%	0.037	5%	7.3	22.7	0.71	32.2	5.9
Average										-	-
Error weighted average										-	-
Carp 68											
p2	1.69E-11	31%	0.004	24%	0.066	3%	15.1	7.0	0.58	11.9	2.8
p3	1.86E-11	11%	0.007	16%	0.060	3%	8.2	7.1	0.57	12.4	4.2
p4[d]	3.37E-11	7%	0.004	26%	0.085	2%	21.7	11.5	0.57	19.9	6.1
Average										12.2	0.3
Error weighted average										12.1	2.3
Carp 67											
p1	2.45E-10	2%	1.218	0%	0.866	0%	0.7	1.4	0.78	1.8	0.2
p2	1.42E-10	3%	0.602	0%	0.643	0%	1.1	1.6	0.77	2.0	0.2
p4[d]	1.19E-11	28%	0.007	17%	0.070	2%	10.2	4.2	0.65	6.4	1.7
p5	5.93E-11	7%	0.245	1%	0.223	1%	0.9	1.6	0.65	2.5	0.5
Average										2.1	0.3
Error weighted average										2.0	0.1
Carp 66											
p1	3.33E-11	12%	0.035	4%	0.183	1%	5.4	3.5	0.56	6.3	4.5
p2[d]	1.00E-10	5%	0.014	9%	0.075	2%	5.5	26.1	0.60	43.3	11.0
p4	5.37E-11	8%	0.097	1%	0.483	0%	5.1	2.1	0.67	3.1	0.5
Average										4.7	2.2
Error weighted average										3.2	0.5
Carp 64											
p1	2.47E-11	17%	0.037	4%	0.117	2%	3.3	3.2	0.60	5.3	1.4
p2	3.74E-11	7%	0.124	1%	0.113	2%	0.9	2.0	0.60	3.4	1.3
p4	4.84E-11	6%	0.162	1%	0.110	2%	0.7	2.1	0.67	3.2	0.4
Average										3.9	1.2
Error weighted average										3.4	0.4
VU Durango											
C11	2.44E-09	0.3%	0.091	2%	2.002	0.1%	22.6	35.6			
C12	1.61E-09	0.6%	0.058	2%	1.335	0.1%	23.8	35.6			
C13	1.14E-09	0.8%	0.044	3%	0.924	0.2%	21.6	35.8			
C14	1.70E-09	0.1%	0.068	2%	1.387	0.1%	20.8	35.2			
C15	1.23E-09	0.2%	0.047	3%	0.981	0.2%	21.5	36.4			
Average							22.0	35.7			
Standard deviation							1.2	0.4			

[a]VU-measurements following procedures of *Foeken et al.* [2003]. ^{4}He abundances were calibrated against an internal ^{4}He standard with a reproducibility of 1.4% (1σ, n = 18, November 2004). Following He-extraction, apatites were prepared for U and Th analyses following procedures of *Foeken et al.* [2003] and spiked with a ^{229}Th/^{233}U spike stock solution.
[b]Blank corrected values; see text for explanation. B.D., below detection limit.
[c]F_T is fraction of alphas retained [*Farley et al.*, 1996]; "corrected ages" are corrected for this effect.
[d]Not taken into account for average and error weighted average.

(RO-11), 9.9 ± 0.8 Ma (RO-04) and 9.2 ± 0.6 Ma (RO-02), suggesting that these were not buried to >60°C since deposition and record provenance ages (Tables 1 and 3).

5.2. Thermal Evolution of the SE Carpathians

[26] Six tectonic units have been identified based on the age data: (1) Crystalline basement and Permo-Mesozoic cover of the Bucovinian nappes, (2) Mesozoic sediments of the Ceahlău unit, (3) Albian–Cenomanian posttectonic cover of the Bucovinian nappes, (4) Cretaceous–Paleogene turbidites of the Miocene external thrust belt, (5) Paleogene–Miocene hinterland sediments of the Transylvania Basin and (6) Upper Miocene–Quaternary postcollisional sediments of the Focşani foredeep basin.

[27] The crystalline basement of the Bucovinian nappes in the Perşani Mountains yields total reset AFT ages of 107 ± 14 (RO-10) and 134 ± 18 Ma (Carp 32) (Figures 3 and 4 and Table 1). A reset AFT age of 107 ± 14 Ma in combination with a negatively skewed MTL of 12.71 ± 0.21 μm (Figure 4b and Table 2) points to a rapid cooling event followed by long residence in the partial annealing zone. Thermal modeling of RO-10, incorporating constraints of the marked Albian unconformity [e.g., *Ştefănescu*, 1976; *Kräutner*, 1980] and the ~9 Ma exhumation of the Transylvania Basin [*Krézsek and Bally*, 2006], suggests Albian cooling at ~7°C/Ma, followed by Paleogene–Miocene reheating and subsequent exhumation to the surface from ~10 Ma onward (Figure 6a and Table 5). In contrast, ages for the Bucovinian basement in the transition zone toward the South Carpathians are much younger. This is indicated by the reset ages of 56 ± 4 (AFT) and 39 ± 6 Ma (AHe) for sample Carp 34 (Figures 3 and 4 and Table 1). Thermal modeling of Carp 34 (Figure 6b and Table 5) suggests that a main cooling event at ~8°C/Ma occurred there from 45 to 33 Ma, suggesting a rapid Eocene cooling event.

[28] Lower Cretaceous conglomerate samples of the Ceahlău unit (Figures 3 and 4 and Table 1, RO-12 and RO-08) yield total reset ages of 49 ± 6 and 13 ± 2 Ma (AFT) and 14 ± 1 Ma (AHe). The younger ages suggest an increase of middle Miocene thermal overprint from the more internal Baraolt nappe toward the more external Ceahlău nappe (Figures 3 and 5). MTLs of 12.93 ± 0.12 μm (RO-12) and 11.73 ± 0.29 μm (RO-08, Table 2) suggest prolonged cooling histories with residence in the partial annealing zone prior to exhumation. Thermal modeling of sample RO-12 (Figure 6c and Table 5), incorporating constraints of the marked unconformities between Turonian–Senonian and Paleogene sediments on top of Lower Cretaceous deposits [e.g., *Săndulescu et al.*, 1981], suggests two main heating-cooling episodes. The first episode is of Eocene age and indicates burial until ~55 Ma, which reached maximum temperatures of ~100°C, followed by cooling from 55 to 50 Ma at a cooling rate of ~13°C/Ma (Figure 6c and Table 5). The second episode shows late Eocene–Oligocene reburial to temperatures of ~80°C followed by cooling from 16 to 9 Ma at a cooling rate of ~8°C/Ma. From 9 Ma to present day, ongoing cooling is recorded at ~2°C/Ma (Figure 6c and Table 5).

[29] The upper Albian–Cenomanian posttectonic cover sealing the Bucovinian nappes yields more disperse reset AFT ages ranging from 93 ± 23 to 50 ± 13 Ma (Figures 3–5 and Table 1; RO-09 and Carp 45), suggesting a Late Cretaceous–Eocene cooling event.

[30] Ages for the Cretaceous–Paleogene turbidites of the Miocene external thrust belt indicate that the area stretching from the Convolute Flysch nappe to the Tarcău nappe was affected by early–middle Miocene exhumation, overprinted by latest Miocene–Pliocene and latest Pliocene–Quaternary exhumation episodes (Table 1 and Figures 3 and 5).

[31] For the internal nappes of the Miocene fold-and-thrust belt (Convolute Flysch, Macla and Audia nappes, Figure 3), AFT reset ages decrease toward the foreland from 19 ± 5, 13 ± 7 and 7 ± 3 Ma (AFT) and 12 ± 2 Ma (AHe) in the Convolute Flysch nappe (Carp 68) to 5 ± 1 Ma (AFT) and 4.3 ± 0.2 Ma (AHe) in the Audia nappe (Carp 31; Figure 5 and Table 1). Thermal modeling of a sample from the Convolute Flysch nappe (Carp 68) suggests rapid middle Miocene cooling (at ~25°C/Ma) from ~90°C to surface temperatures between 13 and 10 Ma (Figure 6d and Table 5). Thermal modeling of a sample from the Audia nappe (Carp 31) indicates the onset of rapid latest Miocene–earliest Pliocene cooling around 6–5 Ma. Cooling occurred in two main pulses (Figure 6e and Table 5); the first pulse occurred between 6 and 4 Ma with cooling from ~110°C to ~55° at a rate of ~33°C/Ma. The second pulse occurred from ~1 Ma to present with cooling from ~55°C to surface temperatures at a rate of ~36°C/Ma.

[32] In the external part of the Miocene fold-and-thrust belt (Tarcău, Marginal Folds and Subcarpathian nappes), AFT ages for the Paleogene sediments of the Tarcău nappe are more dispersed and show a general increase of population ages toward the foreland from reset 11 ± 3 and 3.8 ± 1.6 Ma (RO-07) to reset/nonreset 18 ± 5, 46 ± 11 and 150 ± 62 Ma (RO-05; Figures 3 and 5 and Table 1). Similarly, *Sanders et al.* [1999] obtained AFT age populations of 26 to 20 Ma (early Miocene), 15 to 14 Ma (middle Miocene), 6 to 4 Ma (latest Miocene–early Pliocene) and 2 Ma (latest Pliocene–Quaternary) for samples from the Tarcău nappe (Figures 3 and 5 and Table 1; Carp 64–67). The minimum age populations are apatites least resistant to annealing, which means they are reset around 100–80°C.

[33] Significant latest Pliocene–Quaternary exhumation of the Tarcău nappe is indicated by consistent AHe ages of 3–2 Ma (Figures 3 and 5 and Table 1). Note that these very young exhumation ages are restricted to samples located in the Tarcău nappe with a southeastward shift with respect to the 5 to 4 Ma exhumation ages for the Audia nappe (Figures 3 and 5).

[34] The positively skewed broad track length distribution of RO-07 with a relatively short MTL of 11.62 ± 0.33 μm indicates a complex thermal history with significant partial annealing (Figure 4b). Thermal modeling of this sample, incorporating constraints of the large-scale unconformity observed by late Sarmatian sediments overlying the external part of the Tarcău nappe [e.g., *Murgeanu*, 1967], indicates Paleogene burial up to maximum temperatures of ~110°C, followed by middle Miocene (14–11 Ma) cooling from 108 to 52°C at ~19°C/Ma (Figure 6f and Table 5). After reburial to maximum temperatures of ~100°C, a renewed cooling episode initiated around 3 Ma and yields a significantly higher cooling rate of ~33°C/Ma.

[35] Six AHe samples from the Tarcău nappe have been modeled using their respective single grain AHe ages (Table 5 and Figure 6g). The major model constraint is the late Sarmatian unconformity also described above (box 1). Samples with a post-Sarmatian reset minimum AFT age population (RO-07, Carp 67, Carp 66) are constrained to pass through the 100–80°C isotherm during the timing of the age population (Table 5 and Figure 6g). All model results suggest similar amounts of late Miocene–Pliocene (11–3 Ma) heating (up to ~50°C, Figure 6g), followed by rapid cooling at around 3 Ma at cooling rates of 31 ± 7°C/Ma (average rate of all six samples ± standard deviation, Table 5 and Figure 6g). Interestingly, more internal samples (RO-07, Carp 67, Carp 66) cooled from slightly higher temperatures (~100°C), whereas the more external samples (RO-06, Carp 64, RO-05) cooled from slightly lower temperatures (80–70°C) during post-

Table 5. HeFTy Modeling Constraints and Results[a]

		Modeling Constraints				No. of Paths		AFT Results						AHe Results				Modeling Results					
Sample Code	Tectonic Unit	Box	Constraint	Time (Ma)	Temp. (°C)	Acc	Good	Mod. Age (Ma)	Meas. Age (Ma)	GOF	Mod. L ± SD (μm)	Meas. L ± SD (μm)	GOF	Grain	Mod. AHe (Ma)	Meas. AHe (Ma)	GOF	Timing	C. Rate (°C/Ma)	Ex. Rate (mm/yr)	Error (+/−)	Ex./Bur. (km)	Error (+/−)
RO-10	1) Bucovinian Crystalline bas.	1	AFT age	121–93	120–80	69	0	93.3	105.0	0.37	13.5 ± 1.1	12.7 1.4	0.15	-	-	-	-	Intra-Albian	7	0.4	0.1/0.1	3.2	1.1/0.6
		2	Albian unconf.	112–93	40–5													Paleogene	−1	0.0	0.0/0.0	−2.2	−0.7/0.4
		3	Exhumation TB	12–8	60–5													Late Miocene	6	0.2	0.1/0.0	1.7	0.7/0.4
Carp 34	1) Sub-Bucovinian Crystalline bas.	1	AFT age	60–52	120–80	1452	69	-	-	-	-	-	-	p1	40.6	40.1	0.41	Paleogene	7.5	0.4	0.1/0.1	4.5	1.5/0.9
		2	AHe age	50–33	85–40									p2	40.5	42.3	0.71						
RO-12	2) Baraolt	1	Senonian unconf.	90–80	40–5	7	0	57.2	49.4	0.14	13.1 ± 1.6	12.9 ± 1.2	0.07	p1-S	11.5	12.4	0.08	Intra-Senonian	−2	−0.1	0.0/0.0	−3.5	1.2/0.7
	Lower Cretaceous	2	AFT age	56–46	120–80									p2-S	12.1	12.8	0.19	Paleogene	13	0.7	0.2/0.1	3.3	1.1/0.7
		3	Eocene unconf.	55–45	40–5									p1-L	12.9	13.0	0.95	Early-middle Mio.	8	0.4	0.1/0.1	2.8	0.9/0.6
		4	AHe age	18–12	85–40													Late Miocene	2	0.1	0.0/0.0	0.9	0.3/0.2
Carp 68	4) Convolute Flysch	1	AFT age	20–12	120–80	3591	4245	-	-	-	-	-	-	p2	12.5	12.5	0.98	Early-middle Mio.	25	1.3	0.4/0.3	3.8	1.3/0.8
	Cretaceous	2	AHe age	14–10	85–40									p3	12.5	12.7	0.95	Late Miocene	1	0.1	0.0/0.0	0.3	0.1/0.1
Carp 31	4) Audia nappe	1	AFT age	6–4	120–80	287	6	-	-	-	-	-	-	p1	4.5	4.5	0.89	Pliocene	33	1.7	0.6/0.3	2.7	0.9/0.5
	Cretaceous	2	AHe age	4.7–3.4	85–40									p2	4.3	4.4	0.42	Quaternary	36	1.8	0.6/0.4	2.4	0.8/0.5
														p3	3.8	3.7	0.73						
RO-07	4) Tarcau	1	Stratigraphic age	65–40	15–5	14	0	8.2	7.0	0.14	13.0 ± 2.1	11.6 ± 1.9	0.13	p1-S	2.7	2.8	0.57	Paleogene	−4	−0.2	0.1/0.0	−4.9	1.6/1.0
	Paleogene	2	AFT age pop. 1	14–10	120–80									p3-S	2.7	2.9	0.36	Early-middle Mio.	19	0.9	0.3/0.2	2.8	0.9/0.6
		3	Sarmatian unconf.	12–9	60–5									p1-L	2.8	2.8	0.94	Late Miocene	−7	−0.4	0.1/0.1	−2.8	0.9/0.6
		4	AFT age pop. 2	6–2	120–80									p2-L	2.8	2.8	0.99	Quaternary	33	1.6	0.5/0.3	4.9	1.6/1.0
		5	AHe age	6.0–2.0	85–40																		
Carp 67	4) Tarcau	1	Sarmatian unconf.	12–9	60–5	46	0	-	-	-	-	-	-	p1	2.1	1.8	0.07	Late Miocene	−6	−0.3	0.1/0.1	−2.5	0.8/0.5
	Paleogene	2	AFT age pop. 1	7–5	100–80									p2	2.1	2.2	0.48	Quaternary	41	2.0	0.7/0.4	4.3	1.4/0.9
		3	AFT age pop. 2	3–1	100–80									p5	2.0	2.6	0.07						
		4	AHe age	3.0–1.0	85–40																		
Carp 66	4) Tarcau	1	Sarmatian unconf.	12–9	60–5	3956	84	-	-	-	-	-	-	p1	3.2	7.2	0.34	Late Miocene	−9	−0.4	0.1/0.1	−2.9	1.0/0.6
	Paleogene	2	AFT age	5–3	100–80									p4	3.3	3.3	1.00	Quaternary	27	1.3	0.4/0.3	4.4	1.5/0.9
		3	AHe age	3.6–2.7	85–40																		

Table 5. (continued)

Sample Code	Tectonic Unit	Modeling Constraints: Box	Constraint	Time (Ma)	Temp. (°C)	No. of Paths: Acc	Good	AFT Results: Mod. Age (Ma)	Meas. Age (Ma)	GOF	Mod. L ± SD (μm)	Meas. L ± SD (μm)	GOF	AHe Results: Grain	Mod. AHe (Ma)	Meas. AHe (Ma)	GOF	Modeling Results: Timing	C. Rate (°C/Ma)	Ex. Rate (mm/yr)	Error (+/−)	Ex./Bur. (km)	Error (+/−)
RO-06	4) Tarcau	1	Sarmatian unconf.	12–9	60–5	58	3	-	-	-	-	-	-	p1-S	1.8	1.9	0.39	Late Miocene	−5	−0.2	0.1/0.0	−2.3	0.8/0.5
	Paleogene	2	AHe age	3.0–1.0	85–40									p2-S	1.8	1.7	0.21	Quaternary	38	1.9	0.6/0.4	3.7	1.2/0.7
														p3-S	1.7	1.8	0.73						
														p3-L	1.9	1.9	0.96						
Carp 64	4) Tarcau	1	Sarmatian unconf.	12–9	60–5	955	629	-	-	-	-	-	-	p2	3.1	3.6	0.72	Late Miocene	−6	−0.3	0.1/0.1	−2.0	0.7/0.4
	Paleogene	2	AHe age	3.8–3.0	85–40									p4	3.2	3.2	1.00	Quaternary	24	1.2	0.4/0.2	3.7	1.2/0.7
RO-05	4) Tarcau	1	Sarmatian unconf.	12–9	60–5	267	59	-	-	-	-	-	-	p1-S	3.8	3.8	0.96	Late Miocene	−5	−0.3	0.1/0.1	−2.2	0.7/0.4
	Paleogene	2	AHe age	4.0–2.0	85–40									p2-S	3.7	3.8	0.33	Quaternary	25	1.2	0.4/0.2	3.0	1.0/0.6
														p3-S	3.0	3.0	0.97						

[a]Abbreviations are as follows: No. of paths, number of paths, where the total number of tried paths is 10,000; Acc., number of modeled acceptable paths (0.05 < GOF < 0.5, where GOF is the goodness of fit); good, number of modeled good paths (GOF > 0.5); Mod. age, modeled AFT age; Meas. age, measured AFT age; Mod. L, modeled MTL; SD, standard deviation; Meas. L, measured MTL; Grain, (U-Th)/He single grain ages taken into account for the model; Mod. AHe, modeled (U-Th)/He single grain age; Meas. AHe, measured (U-Th)/He single grain age; C. rate, cooling rate (positive values represent cooling, negative values represent heating); Ex. rate, exhumation rate; Ex./bur., Estimated amounts of exhumation (positive values) or burial (negative values). Exhumation rates and estimates on the amount of exhumation and burial are calculated assuming a constant geothermal gradient of 20 ± 5°C/km, except for the Neogene cooling of sample RO-10 for which a geothermal gradient of 35 ± 10°C/km was adopted (see text for further explanation). Unconf., unconformity; TB, Transylvanian Basin.

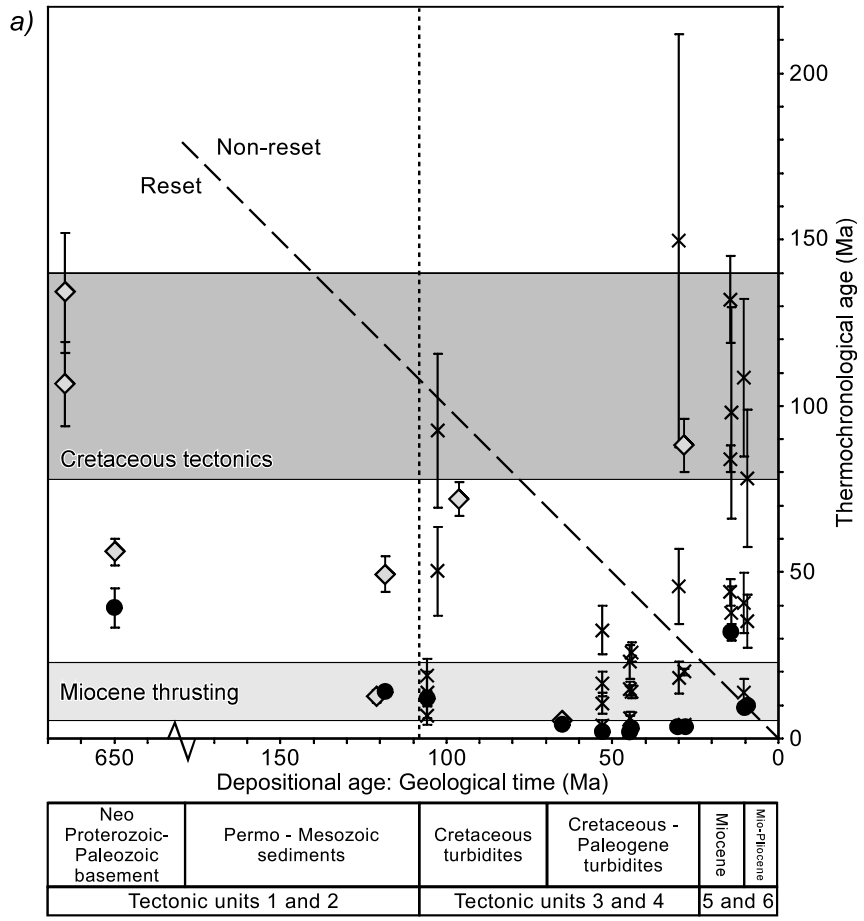

Figure 4a. Thermochronological ages plotted against depositional age. Grey diamonds are AFT central ages and crosses are AFT age populations of this study and *Sanders et al.* [1999]. Solid circles represent error weighted average AHe ages. Ages that fall below the dashed line are reset ages and ages above the dashed line are not reset after deposition and give a provenance age. Samples left of the dotted line are of pre-Albian age and yield total reset ages. Samples to the right of this line are characterized by high AFT age dispersions.

Sarmatian times (Figure 6g). This is reflected by reset and nonreset AFT minimum age populations with respect to the late Sarmatian unconformity for these two groups, respectively (Figure 5).

[36] Oligocene–Miocene hinterland sediments of the Transylvania Basin (Figure 3 and Table 1, RO-11, Carp 47 and Carp 33) yield nonreset AFT ages of 132 ± 13 Ma (Early Cretaceous), 98 ± 32 Ma (Albian–Cenomanian), 88 ± 8 and 84 ± 4 Ma (IntraSenonian) and 44 ± 4 and 38 ± 8 Ma (Eocene). For RO-11, which has a Badenian depositional age (Table 1, 16.4–12.5 Ma), a nonreset AHe age of 32 ± 2 Ma was obtained (Tables 1 and 3). These ages are typical exhumation ages for the basement units (Figure 3 and Table 1) and suggest that the Bucovinian nappes have been a possible source area.

[37] The uppermost Miocene (upper Sarmatian–Meotian) posttectonic cover of the foreland (RO-04 and RO-02) yields AFT provenance ages of 109 ± 24 Ma (Albian), 78 ± 21 Ma (IntraSenonian), 41 ± 9 and 35 ± 8 Ma (Eocene) and 14 ± 4 Ma (middle Miocene) (Figure 5 and Tables 1 and 2). Sample RO-04 with a Meotian depositional age (Table 1, 10.5–8.5 Ma), has a nonreset AHe age of 9.9 ± 0.8 Ma. Sample RO-02 has an AHe age of 9.2 ± 0.6 Ma with single grain ages ranging from 7.4 ± 0.6 to 10.7 ± 2.0 Ma

Figure 4b. (left) The radial plots show AFT single grain ages. Grey shaded area represents the depositional age; Solid black lines indicate central ages for homogeneous samples and age populations for heterogeneous samples (see text for further explanation). Abbreviations: n is number of counted grains; P(χ^2) is probability obtaining Chi-square (χ^2); Ages are central ages (for samples that do not pass P(χ^2) at 5% age is shown in italics); D. is dispersion in single grain ages. (right) The histograms show measured c axis projected confined track lengths. MTL is c axis projected mean track length; SD is standard deviation of track length distribution; n is number of measured horizontal confined tracks.

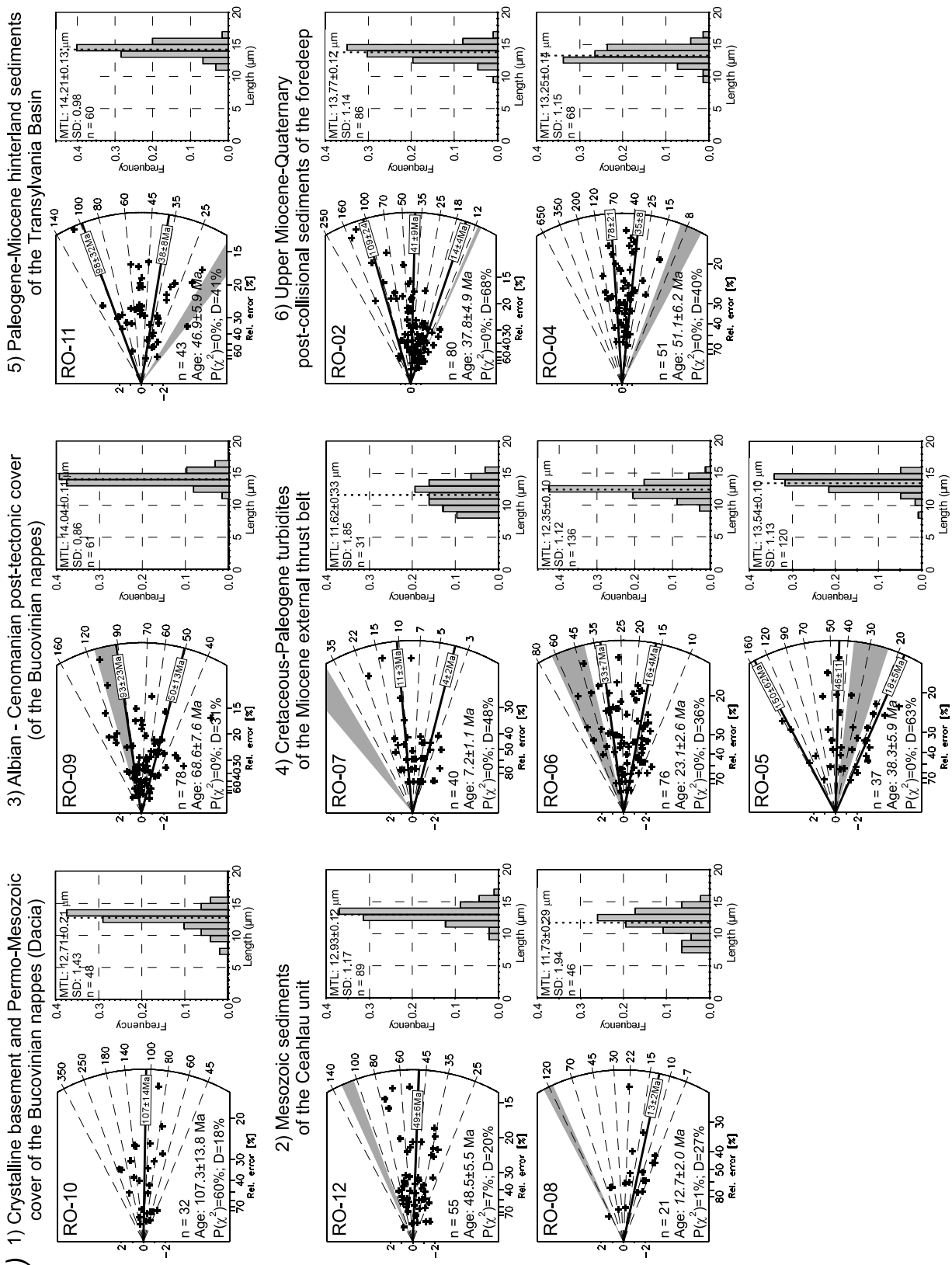
b)
1) Crystalline basement and Permo-Mesozoic cover of the Bucovinian nappes (Dacia)
RO-10
MTL: 12.71±0.21 µm
SD: 1.43
n = 48
107±14Ma
n = 32
Age: 107.3±13.8 Ma
P(χ²)=60%; D=18%
2) Mesozoic sediments of the Ceahlau unit
RO-12
MTL: 12.93±0.12 µm
SD: 1.17
n = 89
49±6Ma
n = 55
Age: 48.5±5.5 Ma
P(χ²)=7%; D=20%
RO-08
MTL: 11.73±0.29 µm
SD: 1.94
n = 46
73±2Ma
n = 21
Age: 12.7±2.0 Ma
P(χ²)=1%; D=27%
3) Albian - Cenomanian post-tectonic cover (of the Bucovinian nappes)
RO-09
MTL: 14.04±0.11 µm
SD: 0.86
n = 61
93±23Ma
60±13Ma
n = 78
Age: 68.6±7.6 Ma
P(χ²)=0%; D=31%
4) Cretaceous-Paleogene turbidites of the Miocene external thrust belt
RO-07
MTL: 11.62±0.33 µm
SD: 1.85
n = 31
11±3Ma
4±2Ma
n = 40
Age: 7.2±1.1 Ma
P(χ²)=0%; D=48%
RO-06
MTL: 12.35±0.10 µm
SD: 1.12
n = 136
33±7Ma
16±4Ma
n = 76
Age: 23.1±2.6 Ma
P(χ²)=0%; D=36%
RO-05
MTL: 13.54±0.10 µm
SD: 1.13
n = 120
160±69Ma
46±11Ma
18±5Ma
n = 37
Age: 38.3±5.9 Ma
P(χ²)=0%; D=63%
5) Paleogene-Miocene hinterland sediments of the Transylvania Basin
RO-11
MTL: 14.21±0.13 µm
SD: 0.98
n = 60
68±32Ma
38±8Ma
n = 43
Age: 46.9±5.9 Ma
P(χ²)=0%; D=41%
6) Upper Miocene-Quaternary post-collisional sediments of the foredeep
RO-02
MTL: 13.77±0.12 µm
SD: 1.14
n = 86
109±24Ma
41±9Ma
14±4Ma
n = 80
Age: 37.8±4.9 Ma
P(χ²)=0%; D=68%
RO-04
MTL: 13.25±0.14 µm
SD: 1.15
n = 68
73±21
35±8
n = 51
Age: 51.1±6.2 Ma
P(χ²)=0%; D=40%
Frequency
Length (µm)
Rel. error [%]

Figure 4b

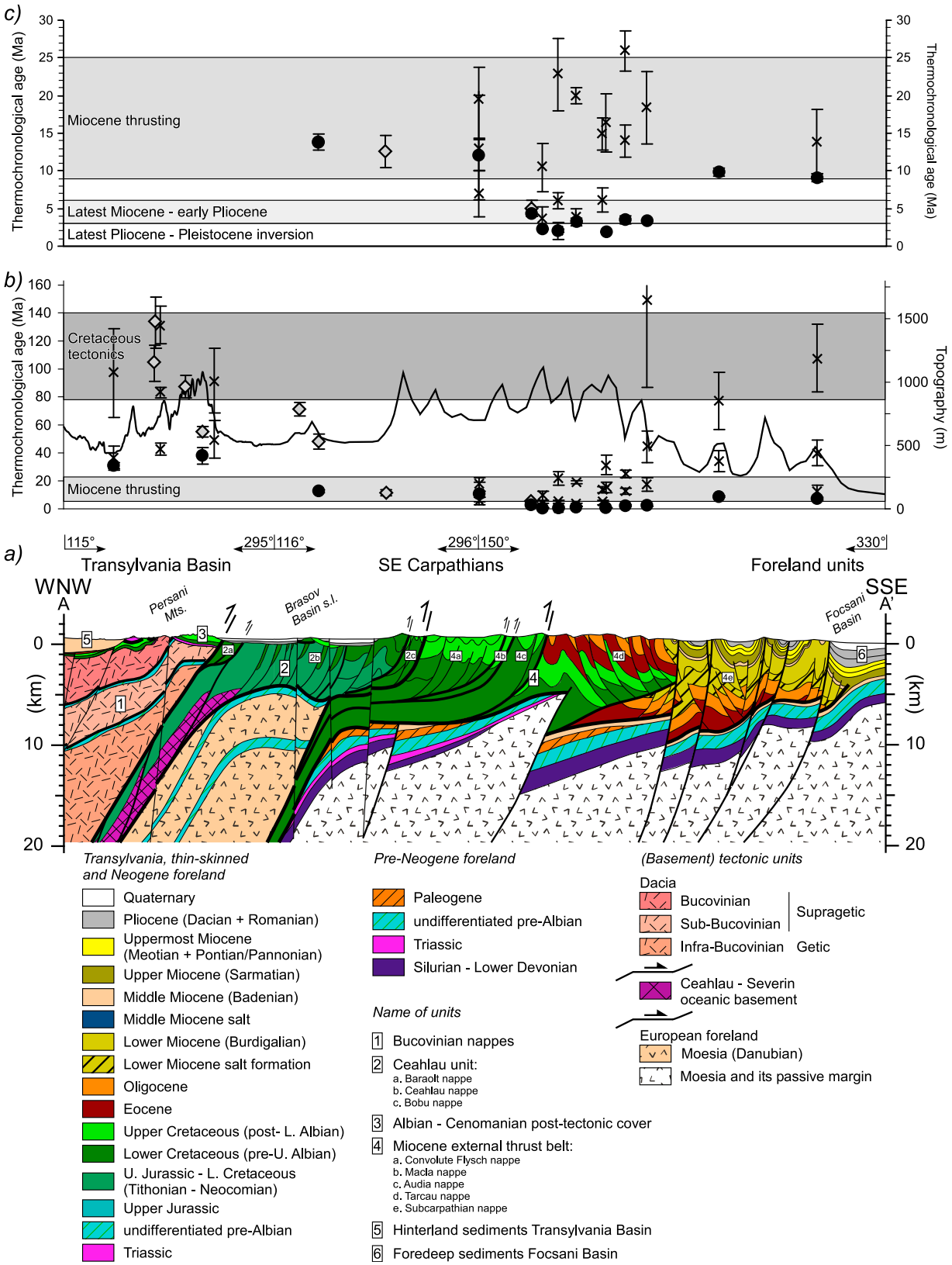
c)
Thermochronological age (Ma)
Thermochronological age (Ma)
Miocene thrusting
Latest Miocene - early Pliocene
Latest Pliocene - Pleistocene inversion
b)
Thermochronological age (Ma)
Topography (m)
Cretaceous tectonics
Miocene thrusting
a)
115°
295°|116°
296°|150°
330°
Transylvania Basin
SE Carpathians
Foreland units
WNW
SSE
A
A'
Persani Mts.
Brasov Basin s.l.
Focsani Basin
(km)
Transylvania, thin-skinned and Neogene foreland
Quaternary
Pliocene (Dacian + Romanian)
Uppermost Miocene (Meotian + Pontian/Pannonian)
Upper Miocene (Sarmatian)
Middle Miocene (Badenian)
Middle Miocene salt
Lower Miocene (Burdigalian)
Lower Miocene salt formation
Oligocene
Eocene
Upper Cretaceous (post- L. Albian)
Lower Cretaceous (pre-U. Albian)
U. Jurassic - L. Cretaceous (Tithonian - Neocomian)
Upper Jurassic
undifferentiated pre-Albian
Triassic
Pre-Neogene foreland
Paleogene
undifferentiated pre-Albian
Triassic
Silurian - Lower Devonian
Name of units
1 Bucovinian nappes
2 Ceahlau unit:
a. Baraolt nappe
b. Ceahlau nappe
c. Bobu nappe
3 Albian - Cenomanian post-tectonic cover
4 Miocene external thrust belt:
a. Convolute Flysch nappe
b. Macla nappe
c. Audia nappe
d. Tarcau nappe
e. Subcarpathian nappe
5 Hinterland sediments Transylvania Basin
6 Foredeep sediments Focsani Basin
(Basement) tectonic units
Dacia
Bucovinian
Sub-Bucovinian
Infra-Bucovinian
Supragetic
Getic
Ceahlau - Severin oceanic basement
European foreland
Moesia (Danubian)
Moesia and its passive margin

Figure 5

(Tables 1 and 3). This is roughly coincident with its upper Sarmatian depositional age, which suggests a short lag time between exhumation of the source and deposition of this sample. The nonreset AFT and AHe ages are typical provenance ages of the orogenic belt (Figure 3 and Table 1), suggesting that the uplifting and eroding middle Miocene orogen might have sourced latest Miocene foredeep sedimentation. The short lag times imply very fast middle–late Miocene erosion of the orogen and subsequent deposition in the adjacent foredeep basin.

6. Interpretation and Estimates on Uplift and Erosion, Subsidence and Sedimentation

[38] The timing and onset of exhumation events coincide with the presence of clastic sediments in the adjacent paleobasins (Cretaceous sediments in the Ceahlău-Severin Ocean, latest Cretaceous–Paleogene sediments in the later Miocene fold-and-thrust belt and post-Sarmatian sediments in the foreland basin), suggesting that post-Jurassic cooling in the SE Carpathians can be ascribed to erosion resulting from either denudation or tectonic uplift. Post-Jurassic heating of rocks can be ascribed to burial by sedimentation. Neogene volcanism in the Perşani Mountains had a negligible effect, as shown by the Cretaceous AFT ages for samples RO-10 and Carp 32 (Figure 3). Minor reheating of the Bucovinian basement rocks surrounding the volcanics in the Perşani Mountains might however explain the relatively short MTL of 12.71 ± 0.21 μm for sample RO-10 (Table 2).

[39] To derive denudation rates from the cooling rates (Table 5 and Figure 7), regional heat flow data [*Veliciu and Visarion*, 1984; *Demetrescu et al.*, 2007] were used to calculate a constant (paleo)-geothermal gradient. The paleo-geothermal gradient is based on the present-day geothermal gradients obtained from the present-day surface heat flow, which is ~40–60 mW/m^2 for the analyzed transect [*Veliciu and Visarion*, 1984; *Demetrescu et al.*, 2001; *Andreescu et al.*, 2002; *Demetrescu et al.*, 2007]. Including thermal conductivities of 1.7–4.5 W/m/°C for the sampled rocks, a paleo-geothermal gradient of 20 ± 5°C/km was calculated for the entire transect. This is in agreement with the modeling of the Miocene thermal evolution of the foreland basin [*Demetrescu et al.*, 2007]. Note that by assuming this relatively low geothermal gradient, amounts and rates of denudation represent maximum estimates. The exception from this calculation is the area close to the Quaternary volcanics of the Perşani Mountains (Figure 3), where a present-day heat flow of ~60–90 mW/m^2 is observed. Thus, a geothermal gradient of 35 ± 10°C/km was adopted for the late Neogene cooling in the Perşani Mountains (sample RO-10).

6.1. Cretaceous–Paleogene Exhumation

[40] Three exhumation phases occurred during Cretaceous–Paleogene times. The intraAlbian ("Austrian") exhumation event recorded the emplacement of the upper Transylvanides nappes, the internal stacking of the basement-bearing Bucovinian nappes and deformation of the most internal thrust sheets of the Ceahlău unit (Figures 8a and 8b). Reset late Early Cretaceous AFT ages obtained for the Bucovinian nappe (RO-10 and Carp 32; Table 1) and thermal modeling suggest intraAlbian exhumation of ~3–5 km (Figures 7 and 8b).

[41] IntraSenonian ("Laramian") exhumation is recorded by Late Cretaceous AFT ages for the Albian–Cenomanian posttectonic cover of the Bucovinian nappes (RO-09 and Carp 45; Table 1) and yields ~3 km of exhumation. It records the internal stacking of the Ceahlău unit and thrusting of the Danubian part of Moesia over the Moesian foreland (Figure 8c).

[42] The Sub-Bucovinian nappe (Carp 34), its Albian–Cenomanian posttectonic cover (RO-09) and the Baraolt nappe (RO-12) experienced early–middle Eocene exhumation of 3–5 km at ~0.4–0.7 mm/yr (Figure 7 and Table 5). Thermal modeling (RO-07) and nonreset Albian and Paleogene detrital AFT ages (RO-05; Table 1) for the Tarcău nappe suggest that this segment of the Carpathians underwent 3.5–5.0 km of coeval burial at ~0.2 mm/yr (Figure 7 and Table 5). A possible source for Paleogene sedimentation in the Carpathian embayment might have been the exhuming Bucovinian–Ceahlău margin (Figure 8d). Paleogene–Miocene burial (~2 km) is also indicated for the Bucovinian basement of the Perşani Mountains at the contact with the Transylvania Basin (Figure 7 and Table 5).

6.2. Miocene Contraction and Collision of the East and SE Carpathian Nappes

[43] The Tisza-Dacia plate started to move into the Carpathian embayment during the Paleogene–early Miocene [e.g., *Csontos*, 1995], subducting the Carpathian embayment and marking the onset of an earlier thrusting epsiode than previously assumed in the Miocene external thrust belt (Figures 8d and 8e). This induced minor exhumation, as indicated by the early Miocene reset AFT age populations in the Convolute Flysch and Tarcău nappes (Table 1). This is in agreement with the posttectonic sediments (the "Doftana molasse") overlying an intraBurdigalian unconformity [e.g., *Ştefănescu and Mărunţeanu*, 1978].

[44] Thrusting resumed during the middle Miocene as indicated by reset AFT and AHe ages of 16–11 Ma (Table 1) and thermal modeling, which suggests 3.2 ± 0.5 km of exhumation (at 0.8 ± 0.4 mm/yr, Figure 7 and Table 5). This is in

Figure 5. (a) Geological cross section of the sample transect (2 × vertical exaggeration, see Figures 1 and 3 for location). Surface structures are obtained from the 1:200,000 map of Romania and cross section X from *Matenco and Bertotti* [2000]. The crustal interpretation is based on the cross section of *Schmid et al.* [2008]. Numbers correspond to the six tectonic units described in the text (also see legend). Subdivisions of groups 2 and 4 indicate the individual nappes of the Ceahlău unit and the Miocene external thrust belt, respectively. (b and c) Thermochronological ages plotted along the sample transect (scale-bar on the left side of the plot; see Figure 4 for explanation of symbols). Solid line is topography (25 × vertical exaggeration; scale-bar on the right side of the plot). Figure 5c is an enlargement of Figure 5b for the Neogene time period to zoom in on the Miocene collisional and subsequent postcollisional exhumation ages.

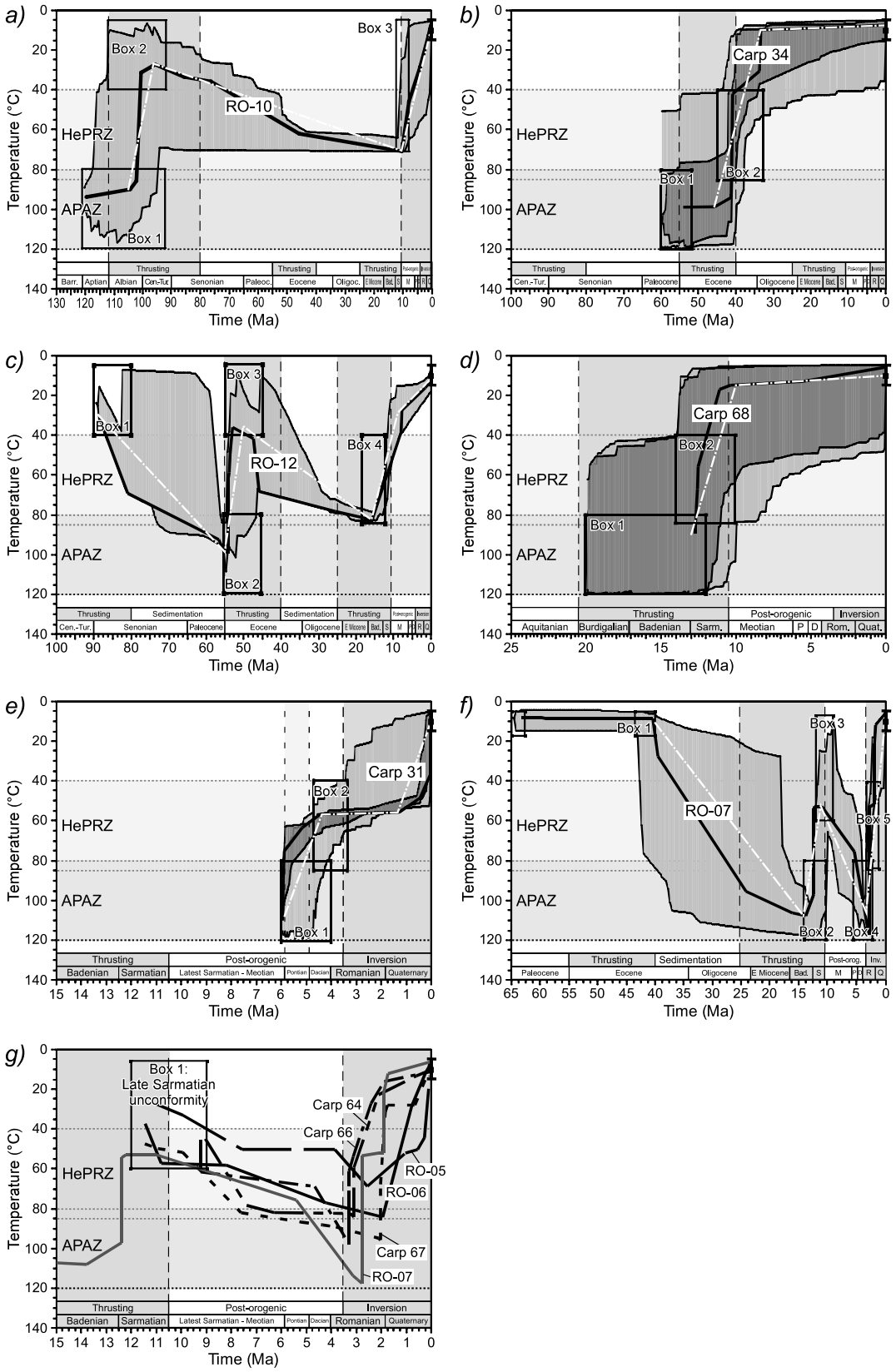
a)
Box 2
Box 3
RO-10
HePRZ
APAZ
Box 1
Temperature (°C)
Time (Ma)
b)
Carp 34
HePRZ
Box 1
Box 2
APAZ
Temperature (°C)
Time (Ma)
c)
Box 3
Box 1
Box 4
RO-12
HePRZ
APAZ
Box 2
Temperature (°C)
Time (Ma)
d)
Carp 68
Box 2
HePRZ
Box 1
APAZ
Temperature (°C)
Time (Ma)
e)
Carp 31
Box 2
HePRZ
APAZ
Box 1
Temperature (°C)
Time (Ma)
f)
Box 1
Box 3
RO-07
Box 5
HePRZ
APAZ
Box 2
Box 4
Temperature (°C)
Time (Ma)
g)
Box 1:
Late Sarmatian
unconformity
Carp 64
Carp 66
RO-05
RO-06
HePRZ
APAZ
Carp 67
RO-07
Temperature (°C)
Time (Ma)

Figure 6

agreement with the ~4 km of exhumation previously reported for the East Carpathians [*Sanders et al.*, 1999; *Gröger et al.*, 2008] and with the age of syntectonic and posttectonic sediments [*Matenco and Bertotti*, 2000; *Săndulescu et al.*, 1981]. Middle Miocene deformation gradually dies out toward the foreland, which is indicated by continuous sedimentation in the Subcarpathian nappe and foredeep. In the Transylvania basin, middle Miocene sediments record AFT and AHe ages that are not reset and are typical for the Bucovinian and Ceahlău units (Table 1), suggesting coeval sourcing by erosional products of this exhumation phase (Figures 7d and 8e).

[45] At the beginning of the late Miocene, the Tarcău nappe was thrusted onto the Moesian foreland together with the Subcarpathian nappe (Figure 8e). Time-temperature histories for the Baraolt, Convolute Flysch and Tarcău nappes (RO-12, Carp 68 and RO-07, Figure 6) indicate that exhumation continued until ~11–9 Ma. This coincides with the widespread latest Miocene–Quaternary unconformable cover of the frontal Carpathian sole thrust [e.g., *Murgeanu*, 1967; *Dumitrescu and Săndulescu*, 1968; *Ştefănescu et al.*, 2000;].

6.3. Late Miocene–Quaternary Postcollisional Evolution

[46] Significant exhumation and deformation occurred in the SE Carpathians after the late Miocene collision. Exhumation in the central part of the nappe system (Audia and Tarcău nappes) is suggested by post–11 Ma AFT and AHe cooling ages and especially by a large number of AHe ages of 3–2 Ma (Table 1). Total postcollisional exhumation is between 2 and 4 km, increasing toward the foreland (Table 5 and Figure 7). This evolution is in strong contrast with the rest of the Carpathians, where no significant deformation/exhumation occurred after the cessation of Miocene thrusting [e.g., *Matenco and Bertotti*, 2000; *Sanders et al.*, 1999].

[47] Based on the new data, the late Miocene to Pleistocene evolution of the SE Carpathians can be subdivided into three periods.

6.3.1. Late Miocene–Early Pliocene: Subsidence of the External Nappes and Foreland Coeval With Hinterland Uplift

[48] Time-temperature models suggest that heating occurred in the Tarcău nappe from 11 to ~3 Ma (Figures 6f and 6g). This is interpreted as heating by sediment burial, which is in the order of 2.4 ± 0.4 km and occurred at a rate of ~0.3 ± 0.1 mm/yr (Figure 7 and Table 5). This is in agreement with regional tectonic reconstructions on the western flank of the Focşani Basin, which have postulated ~2 km of restored sediment thickness over the external nappes [*Leever et al.*, 2006]. Northward and southward, some of the uppermost Miocene sediments still unconformably cover large parts of the Tarcău nappe (Figure 1).

[49] Erosional products from the Miocene orogen are a possible source for latest Miocene clastic sedimentation in the foreland (Figure 8f), as suggested by the nonreset AFT and AHe ages typical of the ones recorded in the orogen (Table 1). The Transylvania Basin, Bucovinian, Ceahlău and Convolute Flysch nappes were slowly exhumed from the late Miocene to present (0.9 ± 0.7 km) at a time integrated exhumation rate of ~0.1 mm/yr (Table 5 and Figures 7 and 8f).

6.3.2. Pliocene–Quaternary Inversion

[50] The new AFT and AHe data suggest that postcollisional exhumation of the Miocene external thrust belt in the SE Carpathians started around 5 Ma. This is compatible with previously reported AFT data [*Sanders et al.*, 1999]. However, the new data allow a significant improvement on spatial and temporal scales and suggest two exhumation episodes for postcollisional times.

[51] Modeled time-temperature histories suggest that the central SE Carpathian orogen (Carp 31, Audia nappe) was exhumed from 6 to 3 Ma (Figure 6e). Exhumation (~2.7 km) occurred rapidly at 1.7 mm/yr (Figure 7 and Table 5). This latest Miocene–early Pliocene exhumation episode, herewith defined as the "first postcollisional exhumation stage," is coeval with the continuation of subsidence in the Tarcău and Subcarpathian nappes (Figure 8g) and the rapid subsidence and sedimentation recorded in the Focşani foredeep [*Leever et al.*, 2006].

[52] AHe ages and thermal models indicate that rapid exhumation occurred at around 3–2 Ma for a large area in the SE Carpathians. This episode, herewith defined as the "second postcollisional exhumation stage," exhumed 3.8 ± 0.9 km of sediments in the Audia and Tarcău nappes from 3 Ma to present at rates of ~1.6 ± 0.3 mm/yr (Figure 7 and Table 5). The Upper Miocene foredeep sediments (RO-04 and RO-02) were exhumed <2 km as suggested by the nonreset AHe ages. The locus of the second postcollisional exhumation stage is shifted toward the foreland by 5–10 km in respect to the

Figure 6. HeFTy model results depicting time-temperature histories (see Table 5 for an overview of modeling constraints and results). The apatite partial annealing zone (APAZ) (120–80°C) and helium partial retention zone (HePRZ) (85–40°C) are shown in grey shades. Black boxes show modeling constraints based on thermochronology results and available geological data (see text for further explanation). All model results are shown as a best fit line (solid black line) as well as a dark-grey and light-grey envelope, encompassing statistically good-fits (GOF > 0.5) and acceptable fits (0.05 < GOF < 0.5), respectively, where GOF is the goodness of fit [*Ketcham*, 2005a]. In deriving cooling rates from the thermal histories, a smoothed version of the modeled best fit thermal history was used (dashed white line). Based on the path envelopes, the uncertainties on the cooling rates are estimated to range from 10–50%, depending on the subsegment. In the discussion of the data, however, no individual uncertainties on cooling rates are reported. Stages and tectonic phases are depicted along the *x* axis. Periods of increased modeled exhumation are highlighted in grey shades. (a) RO-10, crystalline basement of the Bucovinian nappe. (b) Carp 34, crystalline basement of the Sub-Bucovinian nappe. (c) RO-12, Lower Cretaceous sediments of the Ceahlău unit. (d) Carp 68, Cretaceous turbidites of the Convolute Flysch nappe. (e) Carp 31, Upper Cretaceous–Paleogene turbidites of the Audia nappe. (f) RO-07, uppermost Cretaceous-Paleogene turbidites of the Tarcău nappe. (g) Overview of postcollisional evolution of AHe HeFTy model best fit results for all samples from the Tarcău nappe.

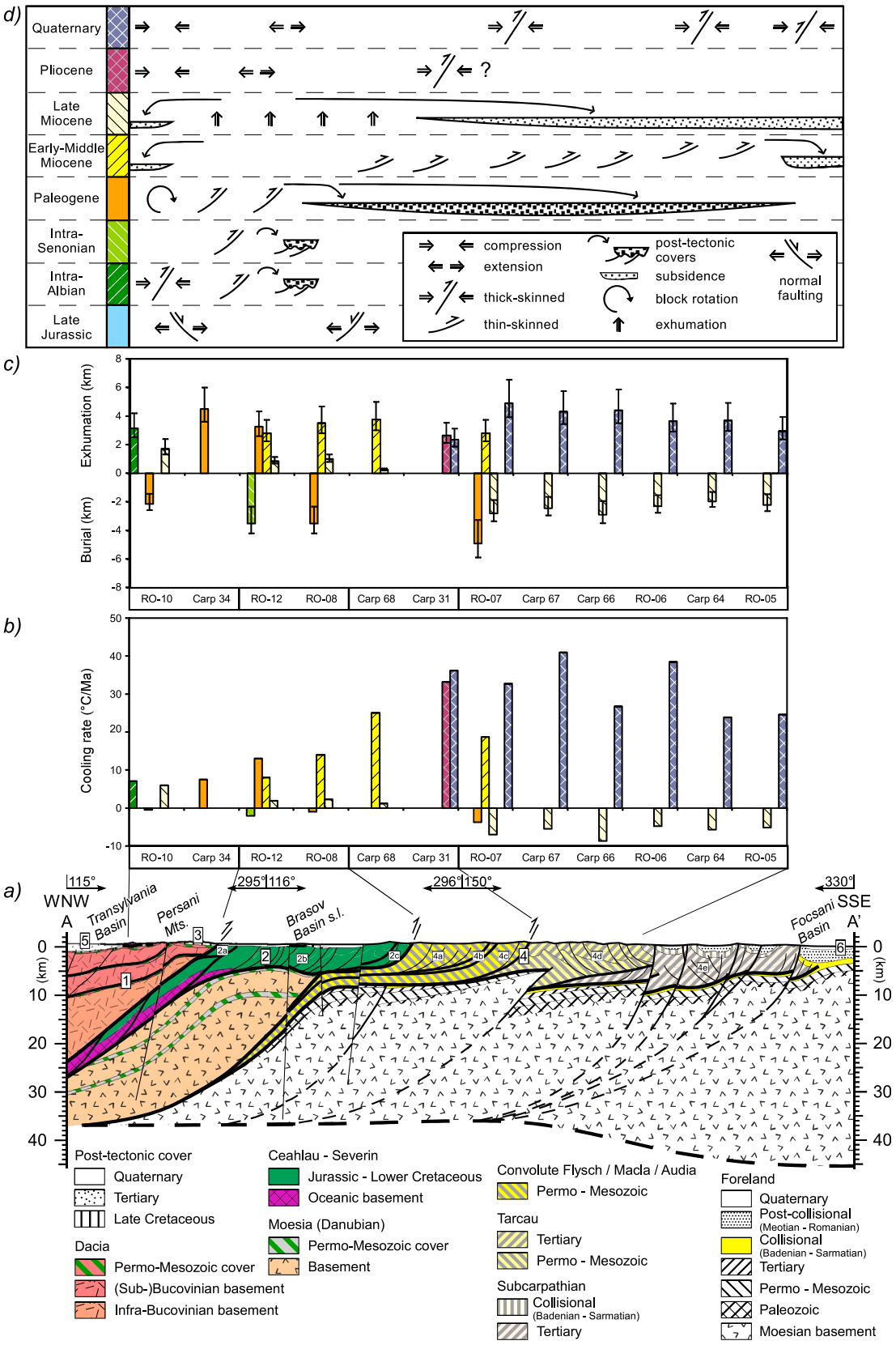
d)
Quaternary
Pliocene
Late Miocene
Early-Middle Miocene
Paleogene
Intra-Senonian
Intra-Albian
Late Jurassic
compression
extension
thick-skinned
thin-skinned
post-tectonic covers
subsidence
block rotation
exhumation
normal faulting
c)
Exhumation (km)
Burial (km)
RO-10 Carp 34 RO-12 RO-08 Carp 68 Carp 31 RO-07 Carp 67 Carp 66 RO-06 Carp 64 RO-05
b)
Cooling rate (°C/Ma)
RO-10 Carp 34 RO-12 RO-08 Carp 68 Carp 31 RO-07 Carp 67 Carp 66 RO-06 Carp 64 RO-05
a)
115°
295°
116°
296°
150°
330°
WNW
A
Transylvania Basin
Persani Mts.
Brasov Basin s.l.
Focsani Basin
SSE
A'
(km)
Post-tectonic cover
Quaternary
Tertiary
Late Cretaceous
Dacia
Permo-Mesozoic cover
(Sub-)Bucovinian basement
Infra-Bucovinian basement
Ceahlau - Severin
Jurassic - Lower Cretaceous
Oceanic basement
Moesia (Danubian)
Permo-Mesozoic cover
Basement
Convolute Flysch / Macla / Audia
Permo - Mesozoic
Tarcau
Tertiary
Permo - Mesozoic
Subcarpathian
Collisional
(Badenian - Sarmatian)
Tertiary
Foreland
Quaternary
Post-collisional
(Meotian - Romanian)
Collisional
(Badenian - Sarmatian)
Tertiary
Permo - Mesozoic
Paleozoic
Moesian basement

Figure 7

previous first postcollisional exhumation stage (Figure 8g). Interestingly, the area for which the youngest AHe ages and largest amount of exhumation were obtained corresponds to the highest present-day elevations (Figure 5), which demonstrates a direct link between recent tectonics and surface topography. The locus of postcollisional exhumation corresponds to the position where the basement beneath the nappe pile is in a shallow position [*Landes et al.*, 2004; *Bocin et al.*, 2005], and is spatially juxtaposed over a shallow Moho configuration [*Hauser et al.*, 2007] (Figure 7). This suggests that postcollisional exhumation is possibly linked to processes taking place at deeper crustal levels.

[53] The second postcollisional exhumation phase suggested by the thermochronological data is corroborated by structural and sedimentological observations. Out-of-sequence thrusting and folding exposed parts of the Subcarpathian nappe buried earlier during the late Miocene–early Pliocene subsidence period (Figures 1a and 5a). Syntectonic sedimentation and coarsening of sedimentary facies are observed for the uppermost Pliocene–Pleistocene [e.g., *Lăzărescu and Popescu*, 1986; *Leever et al.*, 2006; *Jipa*, 2006], such as the deposition of the coarse lower Pleistocene Cîndeşti gravels [*Necea et al.*, 2005].

[54] For the first postcollisional exhumation stage such syntectonic sedimentation patterns are not recorded, suggesting that either tectonics are not responsible for this exhumation phase, or syntectonic sediments were deposited over more internal areas in the orogen and subsequently removed by erosion.

7. Particularities of SE Carpathian Kinematics

[55] Throughout the Late Cretaceous, the Ceahlău-Severin oceanic domain was gradually consumed by subduction starting in intraAlbian times (Figure 8b) and ultimately its sediments were thrust over the thinned European continental passive margin (Figure 8c). Thermochronological ages from the Bucovinian nappe do not show a Senonian overprint, suggesting that the intraAlbian is the major Cretaceous event, recording crustal shortening of the Bucovinian margin enhanced by the collision of the East Vardar ocean and the emplacement of the overlying Transylvanides over hundreds of kilometers [see also *Schmid et al.*, 2008].

7.1. Paleogene Exhumation of the SE Carpathians

[56] There are no posttectonic covers to record the presence of deformation during the entire Paleogene. Based on a gradual eastward transition and thinning of upper Paleocene–lower Eocene sediments from coarse sandstones and conglomerates to more distal facies, *Săndulescu* [1994] has speculated that a low-angle detachment could have been active during this time interval in the depositional domain of the sediments subsequently incorporated in the Tarcău nappe. However, the same arguments could be used for an eastward (in present-day coordinates) thrusting event.

[57] In the South Carpathians, large-scale Paleogene tectonics is known to accommodate the Paleogene–lower Miocene rotation of Tisza-Dacia around Moesia [*Ratschbacher et al.*, 1993], which took place along dextral strike-slip faults with large-offsets (Figure 8d) [*Fügenschuh and Schmid*, 2005]. Since significant early–middle Eocene exhumation is recorded in the transition zone between the South and SE Carpathians, we interpret the Paleogene ages as exhumation related to dextral rotations and translations in the South Carpathians (Figure 8d). In this context, part of the thrusting observed in the Convolute Flysch/Macla/Audia nappes could already have taken place during the Paleogene, the classically defined early Miocene age being only the last peak event. Part of the associated syntectonic sedimentation is still visible in clastic wedges such as the upper Paleocene–lower Eocene one, another part subsequently either removed by erosion or hidden at depth by renewed contraction.

7.2. Collision Mechanics

[58] The SE Carpathians do not show enhanced exhumation in the upper plate (the Bucovinian basement) during collision, in contrast with theoretical models of retroshear exhumation of double-vergent orogenic wedges [e.g., *Beaumont et al.*, 1994; *Schmid et al.*, 1996; *Willett and Brandon*, 2002]. This is demonstrated by the fact that the exhumation of the Bucovinian basement and the neighboring Transylvania Basin at around 9 Ma [*Krézsek and Bally*, 2006] was minor and exhumation was not enough to reset AFT ages (Figures 7 and 8e). One alternative explanation for minor exhumation of the orogenic core is the possibility that the subduction zone has shifted toward the foreland, i.e., beneath the Danubian part of the Moesian platform (Figure 7a) accreted to the upper plate at the end of the Cretaceous (Figures 8c and 8e). This is in agreement with similar kinematics of the South Carpathians [see *Fügenschuh and Schmid*, 2005].

[59] The amount of exhumation related to Miocene nappe stacking and collision is roughly similar across the Ceahlău unit and Miocene external thrust belt (Figures 7 and 8e). The final moment of collision is still recorded, as thermal modeling indicates some acceleration of exhumation around 12–11 Ma (Figure 6).

Figure 7. (a) Tectonic cross section of the sample transect (see Figures 1 and 3 for location). Surface structures are obtained from *Săndulescu* [1984] and cross-section X from *Matenco and Bertotti* [2000]. The crustal interpretation is based on the cross section of *Schmid et al.* [2008]. Dashed line at 30–40 km depth represents Moho depth extrapolated from *Hauser et al.* [2007]. Numbers correspond to the six tectonic units described in the text (see Figure 5a for legend). (b) Overview of cooling rates and (c) estimated amounts of exhumation and burial for the modeled samples from NW to SE. The colors indicate the main phases from Late Jurassic to Quaternary as obtained from the time-temperature models and known tectonic phases (see Figure 7d for legend). Geothermal gradient is 20°C/km and error bars represent values for geothermal gradients of 25 and 15°C/km. (d) Interpretation of the obtained exhumation episodes. See text for further explanation.

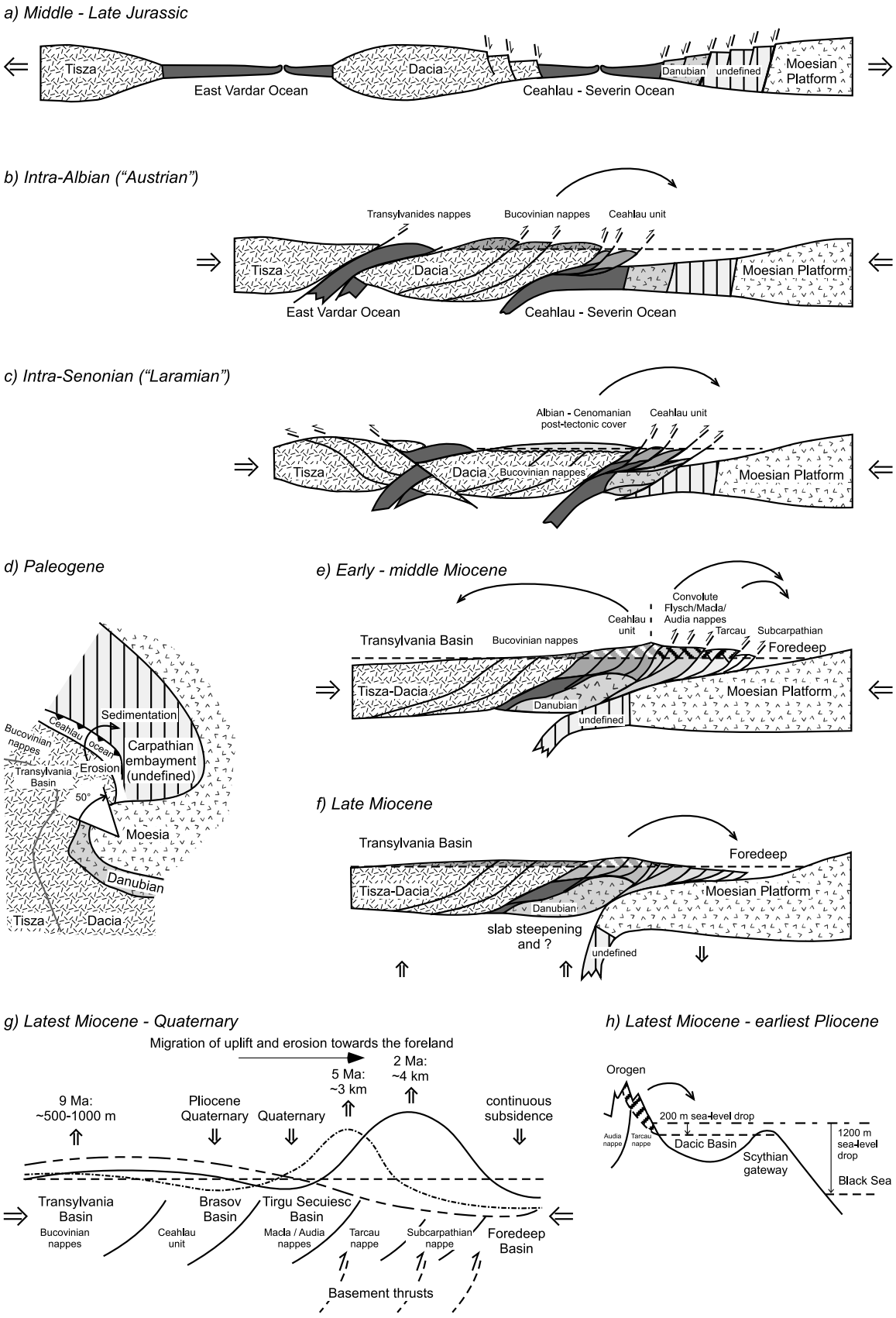
a) Middle - Late Jurassic
Tisza
East Vardar Ocean
Dacia
Ceahlau - Severin Ocean
Danubian
undefined
Moesian Platform
b) Intra-Albian ("Austrian")
Transylvanides nappes
Bucovinian nappes
Ceahlau unit
Tisza
Dacia
Moesian Platform
East Vardar Ocean
Ceahlau - Severin Ocean
c) Intra-Senonian ("Laramian")
Albian - Cenomanian post-tectonic cover
Ceahlau unit
Tisza
Dacia
Bucovinian nappes
Moesian Platform
d) Paleogene
Sedimentation
Ceahlau ocean
Bucovinian nappes
Carpathian embayment (undefined)
Erosion
Transylvania Basin
50°
Moesia
Danubian
Tisza
Dacia
e) Early - middle Miocene
Convolute Flysch/Macla/ Audia nappes
Ceahlau unit
Tarcau
Subcarpathian
Transylvania Basin
Bucovinian nappes
Foredeep
Tisza-Dacia
Moesian Platform
Danubian
undefined
f) Late Miocene
Transylvania Basin
Foredeep
Tisza-Dacia
Moesian Platform
Danubian
slab steepening and ?
undefined
g) Latest Miocene - Quaternary
Migration of uplift and erosion towards the foreland
9 Ma: ~500-1000 m
Pliocene Quaternary
Quaternary
5 Ma: ~3 km
2 Ma: ~4 km
continuous subsidence
Transylvania Basin
Bucovinian nappes
Brasov Basin
Ceahlau unit
Tirgu Secuiesc Basin
Macla / Audia nappes
Tarcau nappe
Subcarpathian nappe
Foredeep Basin
Basement thrusts
h) Latest Miocene - earliest Pliocene
Orogen
200 m sea-level drop
Audia nappe
Tarcau nappe
Dacic Basin
Scythian gateway
1200 m sea-level drop
Black Sea

Figure 8

7.3. Postcollisional Exhumation and Subsidence: What Is Driving It?

[60] The new AFT and AHe data demonstrate that the SE Carpathians are characterized by two postcollisional exhumation stages. Clear tectonic links have been identified for the second postcollisional exhumation stage. The latter stage is characterized by coeval uplift and subsidence and is the result of a tectonic episode which differs from the early to middle Miocene nappe stacking. The back-stepping of the center of maximum exhumation, the correlation between the uplift and erosion of the nappe pile and the shallow basement/Moho (Figure 7), and the out-of-sequence deformation mode suggest generalized crustal-scale uplift beneath the orogen coeval with foreland subsidence. The ~5 km Quaternary shortening suggested in recent studies by seismic analysis and geomorphological analysis of river terraces [e.g., *Necea et al.*, 2005; *Leever et al.*, 2006] is similar in magnitude to the total amount of denudation obtained for the external nappes (3.8 ± 0.9 km). Shortening along steep basement thrusts would yield comparable vertical magnitudes with respect to the amount of uplift and erosion. Therefore, the second postcollisional exhumation stage is interpreted to be related to reverse faulting along basement thrusts and the subsequent erosion of the uplifted areas (Figure 8g). When combined with the subsidence in the foreland, this gives a fold-like geometry at crustal scale (Figure 8g). This type of strain partitioning in the foreland of an orogen is a known process, defined as collisional coupling by *Ziegler et al.* [1995].

[61] The first postcollisional exhumation stage may be interpreted following two possible scenarios. The first scenario (Figure 8g) assumes a tectonic uplift of the thin-skinned nappe pile and can justify the shift from internal to external sediment sources observed in the SE Carpathians at 5–6 Ma [*Panaiotu et al.*, 2007]. If this tectonically driven scenario is assumed, a lateral migration of exhumation and an increase in amplitudes from the hinterland toward the foreland can be observed in the SE Carpathians during the entire postcollisional time interval (Figure 8g). At first, the margin of the Transylvania basin adjacent to the SE Carpathians was exhumed at the end of the Pannonian times (~9 Ma). Subsequently, the locus of exhumation migrated in time to the limit between the Audia and Tarcău nappes at 5–6 Ma (first postcollisional exhumation stage) and then more to the foreland in the center of the Tarcău nappe starting around 3–2 Ma (second postcollisional exhumation stage). The amplitudes of exhumation are also increasing in time, from <2 km at the end of the Pannonian, to ~2.7 km in the Pliocene, reaching 3.8 km during the Quaternary with similar rates of exhumation for the last two episodes (~1.6–1.7 mm/yr). In terms of deep lithospheric mechanics, any of the Vrancea slab models which assume the coupling with uplift in the orogen and subsidence driven by the slab pull in the foreland, migrating in time after the collision can be discussed in this context. These models include, although not exclusively, a gravitational instability of the mantle lithosphere [*Houseman and Gemmer*, 2007], delamination [e.g., *Knapp et al.*, 2005] or lithospheric folding conditioned by the slab pull [*Matenco et al.*, 2007].

[62] In the second, more speculative, scenario (Figure 8h), the first postcollisional exhumation stage is associated with a base-level drop and rapid fill observed in the Carpathian foreland after 6 Ma [*Leever*, 2007] related to the large-scale sea level drop of the Messinian Salinity Crisis (MSC, 5.96–5.33 Ma) [*Krijgsman et al.*, 1999]. Recent studies of orogenic evolution in the Mediterranean realm, such as for the Alps [e.g., *Willett et al.*, 2006], indicated a shift of exhumation to orogenic interiors and a change to orogenic destruction coeval with the MSC. This induced erosion given by larger exposures of the Mediterranean domain during the Messinian low stand [e.g., *Clauzon et al.*, 1996; *Foeken et al.*, 2003]. These conditions are met in a similar fashion for the orogens in the Paratethys realms such as the SE Carpathians, where a coeval large sea level drop associated with massive sedimentation has been reported for the Black Sea [see *Dinu et al.*, 2005; *Gillet et al.*, 2007]. This MSC middle Pontian sea level drop recorded in the Paratethys domain [e.g., *Stoica et al.*, 2007] has potentially induced a shift of depocenters toward the deeper parts of the Black Sea, which is coeval with enhanced erosion of the orogen and exposed parts of the basins.

8. Conclusions

[63] AFT and AHe thermochronology indicate an exhumation history for the SE Carpathians which covers their entire contractional evolution, from the onset of nappe stacking in the Cretaceous to the recent postcollisional deformations. This is a significant improvement of the qualitative averaging results of previous AFT studies [e.g., *Sanders et al.*, 1999]. Cooling ages generally decrease from Cretaceous for the internal basement nappes (AFT and AHe ages), to Miocene–Quaternary (AFT and AHe, respectively) toward the foreland, confirming the idea of a forward breaking sequence of the contractional episodes, which generally

Figure 8. Schematic sketches illustrating the Jurassic to present-day evolution of the SE Carpathians. Dashed horizontal line in cross sections (Figures 8a–8c and 8e–8h) depicts estimated base-level. Shades above base-level are eroding areas as estimated from the thermochronology results. Arrows indicate interpreted sediment migration. Schematic cross sections are modified after *Schmid et al.* [2008]. (a) Middle–Late Jurassic exhumation: tectonic unroofing due to rifting of the Ceahlău-Severin Ocean. (b) IntraAlbian exhumation: onset of contraction in the SE Carpathians. (c) IntraSenonian exhumation: ongoing contraction. (d) Paleogene exhumation: shortening induced by dextral rotations around the Moesian promontory [modified after *Schmid et al.*, 1998]. (e) Early–middle Miocene exhumation: thrusting and subsequent erosion induced by ongoing shortening. (f) Late Miocene: uplift of the Transylvania hinterland and internal nappes coeval with rapid subsidence in the external SE Carpathians and foredeep. (g) Latest Miocene–Quaternary: foreland propagating center of maximum exhumation. (h) Alternative interpretation for the first postcollisional exhumation stage: increased erosion by a base-level drop due to the MSC. See text for further explanation.

overlap classical tectonic stages defined by field kinematics.

[64] The most significant Cretaceous event is the intraAlbian exhumation (~3–5 km) related to the continental collision of the East Vardar Ocean, thick-skinned shortening of the Bucovinian nappes and the onset of subduction of the Ceahlău-Severin ocean. The upper plate of the Ceahlău-Severin subduction (i.e., the Bucovinian basement) has not been exhumed at AFT resolution since the intraAlbian event. Rather limited intraSenonian exhumation (~3 km) is related to the subduction of the oceanic part of the Ceahlău-Severin Ocean and possibly the thrusting of its sediments over the European continental passive margin. Exhumation rates of 0.4–0.7 mm/yr obtained for the Paleogene can be related to an earlier onset of thrusting in the internal nappes of the Miocene external thrust belt of the East and SE Carpathians, associated with the rotation of Tisza-Dacia around the Moesian promontory.

[65] The new data furthermore suggest that the SE Carpathians have been affected by early–middle Miocene exhumation of 3.2 ± 0.5 km, which occurred at rates of 0.8 ± 0.4 mm/yr. These exhumation rates are similar to the one previously inferred for the East Carpathians [*Sanders et al.*, 1999]. After the Sarmatian collision, the hinterland (Transylvania Basin, Bucovinian nappes and Ceahlău unit) was gradually uplifted and eroded at slow rates of ~0.1 mm/yr (0.8 ± 0.4 km).

[66] In contrast to the rest of the Romanian Carpathians, the SE Carpathian tectonic evolution is overprinted by two younger exhumation events in the Pliocene–Pleistocene. The first postcollisional exhumation phase (latest Miocene–early Pliocene) in the central part of the Miocene external thrust belt occurred at high exhumation rates (~1.7 mm/yr), and is interpreted as a tectonic event and/or associated with a sea level drop in the Paratethys basins during the Messinian low stand. The second postcollisional exhumation phase suggests rapid Pleistocene exhumation (3.8 ± 0.9 km at rates of 1.6 ± 0.3 mm/yr) for the external part of the Miocene thrust belt and is interpreted to represent crustal-scale shortening by reverse faulting along steep basement thrusts and the subsequent erosion of the uplifted areas.

[67] The evolution of the SE Carpathians represents an effect of the interplay between orogenic and intraplate processes conditioned by the late-stage evolution of the Vrancea slab. Data suggest that the SE Carpathians did not develop as a typical double-vergent orogenic wedge; instead, exhumation was related to a foreland-vergent sequence of nappe stacking during collision and was subsequently followed by a large out-of-sequence shortening event truncating the already locked collisional boundary.

[68] **Acknowledgments.** This research forms part of the Pannonian–Carpathians program of the Netherlands Research Centre for Integrated Solid Earth Science (ISES). Travel costs for He-measurements at SUERC (UK) were funded by the Ph.D. fund of the Faculty of Earth and Life Sciences (VU University, Amsterdam). Roel van Elsas, Tineke Vogel-Eissens, Joaquim Juez-Larré, David Vilbert and Bas van der Wagt are thanked for help and assistance in mineral separation procedures, fission track preparation, He-measurements and ICP-MS analyses. Two anonymous reviewers are thanked for their constructive and detailed suggestions, which have significantly improved the manuscript. This is contribution 20091101 of the Netherlands Research School of Sedimentary Geology (NSG).

References

Andreescu, M., S. B. Nielsen, G. Polonic, and C. Demetrescu (2002), Thermal budget of the Transylvanian lithosphere. Reasons for a low surface heat-flux anomaly in a Neogene intra-Carpathian basin, *Geophys. J. Int.*, *150*(2), 494–505, doi:10.1046/j.1365-246X.2002.01724.x.

Balestrieri, M. L., F. M. Stuart, C. Persano, E. Abbate, and G. Bigazzi (2005), Geomorphic development of the escarpment of the Eritrean margin, southern Red Sea from combined apatite fission-track and (U-Th)/He thermochronometry, *Earth Planet. Sci. Lett.*, *231*, 97–110, doi:10.1016/j.epsl.2004.12.011.

Balla, Z. (1987), Tertiary paleomagnetic data for the Carpatho-Pannonian region in the light of Miocene rotation kinematics, *Tectonophysics*, *139*, 67–98, doi:10.1016/0040-1951(87)90198-3.

Barbarand, J., T. Hurford, and A. Carter (2003), Variation in apatite fission-track length measurement: Implications for thermal history modelling, *Chem. Geol.*, *198*, 77–106, doi:10.1016/S0009-2541(02)00423-0.

Beaumont, C. (1981), Foreland basins, *Geophys. J. R. Astron. Soc.*, *56*, 291–329.

Beaumont, C., P. H. Fullsack, and J. Hamilton (1994), Styles of crustal deformation in compressional orogens caused by subduction of the underlying lithosphere, *Tectonophysics*, *232*, 119–132, doi:10.1016/0040-1951(94)90079-5.

Bertotti, G., L. Matenco, and S. Cloetingh (2003), Vertical movements in and around the south-east Carpathian foredeep: Lithospheric memory and stress field control, *Terra Nova*, *15*, 299–305, doi:10.1046/j.1365-3121.2003.00499.x.

Bertotti, G., P. Mosca, J. Juez, R. Polino, and T. Dunai (2006), Oligocene to Present kilometres scale subsidence and exhumation of the Ligurian Alps and the Tertiary Piedmont Basin (NW Italy) revealed by apatite (U–Th)/He thermochronology: Correlation with regional tectonics, *Terra Nova*, *18*, 18–25, doi:10.1111/j.1365-3121.2005.00655.x.

Bocin, A., R. Stephenson, A. Tryggvason, I. Panea, V. Mocanu, F. Hauser, and L. Matenco (2005), 2.5D seismic velocity modelling in the southeastern Romanian Carpathians Orogen and its foreland, *Tectonophysics*, *410*, 273–291, doi:10.1016/j.tecto.2005.05.045.

Brandon, M. T. (1992), Decomposition of fission-track grain-age distributions, *Am. J. Sci.*, *292*, 535–564.

Brandon, M. T. (2002), Decomposition of mixed grain-age distributions using BINOMFIT, *On Track*, *24*, 13–18.

Brandon, M. T., M. K. Roden-Tice, and J. I. Garver (1998), Late Cenozoic exhumation of the Cascadia accretionary wedge in the Olympic Mountains, NW Washington State, *Geol. Soc. Am. Bull.*, *110*, 985–1009, doi:10.1130/0016-7606(1998)110<0985:LCEOTC>2.3.CO;2.

Carlson, W. D., R. A. Donelick, and R. A. Ketcham (1999), Variability of apatite fission-track annealing kinetics: I. Experimental results, *Am. Mineral.*, *84*, 1213–1223.

Clauzon, G., J.-P. Suc, F. Gautier, A. Berger, and M.-F. Loutre (1996), Alternate interpretation of the Messinian salinity crisis: Controversy resolved?, *Geology*, *24*, 363–366, doi:10.1130/0091-7613(1996)024<0363:AIOTMS>2.3.CO;2.

Cloetingh, S., E. Burov, L. Matenco, G. Toussaint, G. Bertotti, P. A. M. Andriessen, M. J. R. Wortel, and W. Spakman (2004), Thermo-mechanical controls on the mode of continental collision in the SE Carpathians (Romania), *Earth Planet. Sci. Lett.*, *218*(1–2), 57–76, doi:10.1016/S0012-821X(03)00645-9.

Csontos, L. (1995), Tertiary evolution of the Intracarpathian area: A review, *Acta Vulcanol.*, *7*, 1–15.

Csontos, L., and A. Vörös (2004), Mesozoic plate tectonic reconstruction of the Carpathian region, *Palaeogeogr. Palaeoclimatol. Palaeoecol.*, *210*(1), 1–56, doi:10.1016/j.palaeo.2004.02.033.

Demetrescu, C., S. B. Nielsen, M. Ene, D. Z. Şerban, G. Polonic, M. Andreescu, A. Pop, and N. Balling (2001), Lithosphere thermal structure and evolution of the Transylvanian Depression–Insights from new geothermal measurements and modelling results, *Phys. Earth Planet. Inter.*, *126*, 249–267, doi:10.1016/S0031-9201(01)00259-X.

Demetrescu, C., H. Wilhelm, M. Tumanian, S. B. Nielsen, A. Damian, V. Dobrică, and M. Ene (2007), Time-dependent thermal state of the lithosphere in the foreland of the Eastern Carpathians bend. Insights from new geothermal measurements and modeling results, *Geophys. J. Int.*, *170*, 896–912, doi:10.1111/j.1365-246X.2007.03408.x.

Dinu, C., H. K. Wong, D. Tambrea, and L. Matenco (2005), Stratigraphic and structural characteristics of the Romanian Black Sea shelf, *Tectonophysics*, *410*, 417–435, doi:10.1016/j.tecto.2005.04.012.

Donelick, R. A. (1993), Apatite etching characteristics versus chemical composition, *Nucl. Tracks Radiat. Meas.*, *21*, 604, doi:10.1016/1359-0189(93)90241-Z.

Donelick, R. A., and D. S. Miller (1991), Enhanced TINT fission track densities in low spontaneous track density apatites using ^{252}Cf-derived fission fragment tracks: A model and experimental observations, *Nucl. Tracks Radiat. Meas.*, *18*(3), 301–307, doi:10.1016/1359-0189(91)90022-A.

Donelick, R. A., R. A. Ketcham, and W. D. Carlson (1999), Variability of apatite fission-track annealing kinetics II: Crystallographic orientation effects, *Am. Mineral.*, *84*, 1224–1234.

Dumitrescu, F., and M. Săndulescu (1968), Problèmes structuraux fondamentaux des Carpathes roumains et de leur Avant-pays, *Ann. Com. Geol. Rom.*, *36*, 195–218.

Dunkl, I. (2000), Trackkey: A windows program for calculation and graphical presentation of fission track data, *Comput. Geosci.*, *28*, 3–12.

Ehlers, T. A., et al. (2005), Computational tools for low-temperature thermochronometer interpretation, *Rev. Mineral. Geochem.*, *58*, 589–622, doi:10.2138/rmg.2005.58.22.

Faccenna, C., C. Piromallo, A. Crespo-Blanc, L. Jolivet, and F. Rosetti (2004), Lateral slab deformation and the origin of the western Mediterranean arcs, *Tectonics*, *23*, TC1012, doi:10.1029/2002TC001488.

Farley, K. A. (2000), Helium diffusion from apatite: General behavior as illustrated by Durango fluorapatite, *J. Geophys. Res.*, *105*(B2), 2903–2914, doi:10.1029/1999JB900348.

Farley, K. A. (2002), (U-Th)/He dating; techniques, calibrations, and applications, in *Noble Gases in Geochemistry and Cosmochemistry*, *Rev. Mineral. Geochem.*, vol. 47, edited by D. Porcelli, C. J. Ballentine and R. Wieler, pp. 819–843, Mineral. Soc. of Am., doi:10.2138/rmg.2002.47.18.

Farley, K. A., R. A. Wolf, and L. T. Silver (1996), The effects of long alpha-stopping distances on (U-Th)/He ages, *Geochim. Cosmochim. Acta*, *60*, 4223–4229, doi:10.1016/S0016-7037(96)00193-7.

Foeken, J., T. Dunai, G. Bertotti, and P. Andriessen (2003), Late Miocene to Present exhumation in the Ligurian Alps (SW Alps) with evidence for accelerated denudation during the Messinian Salinity Crisis, *Geology*, *31*, 797–800, doi:10.1130/G19572.1.

Foeken, J. P. T., F. M. Stuart, K. J. Dobson, C. Persano, and D. Vilbert (2006), A diode laser system for heating minerals for (U-Th)/He chronometry, *Geochem. Geophys. Geosyst.*, *7*, Q04015, doi:10.1029/2005GC001190.

Fügenschuh, B., and S. M. Schmid (2005), Age and significance of core complex formation in a very curved orogen: Evidence from fission track studies in the South Carpathians (Romania), *Tectonophysics*, *404*(1–2), 33–53, doi:10.1016/j.tecto.2005.03.019.

Galbraith, R. F. (1981), On statistical models for fission track counts, *Math. Geol.*, *13*(6), 471–478, doi:10.1007/BF01034498.

Galbraith, R. F., and G. M. Laslett (1993), Statistical models for mixed fission track ages, *Nucl. Tracks*, *5*, 3–14.

Gillet, H., G. Lericolais, and J.-P. Rehault (2007), Messinian event in the black sea: Evidence of a Messinian erosional surface, *Mar. Geol.*, *244*(1–4), 142–165, doi:10.1016/j.margeo.2007.06.004.

Gleadow, A. J. W., and I. R. Duddy (1981), A natural long-term annealing experiment for apatite, *Nucl. Tracks Radiat. Meas.*, *5*, 169–174.

Gradstein, F. M., J. G. Ogg, A. G. Smit, W. Bleeker, and L. J. Lourens (2004), A new geological time scale with special references to Precambrian and Neogene, *Episodes*, *27*(2), 83–100.

Gröger, H. R., B. Fügenschuh, M. Tischler, S. M. Schmid, and J. P. T. Foeken (2008), Tertiary cooling and exhumation history in the Maramures area (internal eastern Carpathians, northern Romania): Thermochronology and structural data, in *Tectonic Aspects of the Alpine-Dinaride-Carpathian System*, edited by S. Siegesmund, B. Fügenschuh, and N. Froitzheim, *Geol. Soc. Spec. Publ.*, *298*, 169–195, doi:10.1144/SP298.9.

Haq, B., J. Hardenbol, and P. Vail (1987), Chronology of fluctuating sea level since Triassic (250 million years to present), *Science*, *235*, 1156–1167, doi:10.1126/science.235.4793.1156.

Hauser, F., V. Raileanu, W. Fielitz, C. Dinu, M. Landes, A. Bala, and C. Prodehl (2007), Seismic crustal structure between the Transylvanian Basin and the Black Sea, Romania, *Tectonophysics*, *430*, 1–25, doi:10.1016/j.tecto.2006.10.005.

Hippolyte, J.-C., and M. Săndulescu (1996), Paleostress characterization of the "Wallachian" phase in its type area (southeastern Carpathians, Romania), *Tectonophysics*, *263*, 235–248, doi:10.1016/S0040-1951(96)00041-8.

Houseman, G. A., and L. Gemmer (2007), Intra-orogenic extension driven by gravitational instability: Carpathian-Pannonian orogeny, *Geology*, *35*(12), 1135–1138, doi:10.1130/G23993A.1.

Hurford, A. J., and P. F. Green (1982), A user's guide to fission track dating calibration, *Earth Planet. Sci. Lett.*, *59*, 343–354, doi:10.1016/0012-821X(82)90136-4.

Hurford, A. J., and P. F. Green (1983), The Zeta age calibration of fission-track dating, *Isot. Geosci.*, *1*, 285–317.

Jipa, D. (2006), *Bazinul Dacic: Arhitectură Sedimentară, Evoluție, Factori de Control*, 306 pp., GeoEcoMar, Bucharest.

Jolivet, L., and C. Faccenna (2000), Mediterranean extension and the Africa-Eurasia collision, *Tectonics*, *19*, 1095–1106, doi:10.1029/2000TC900018.

Ketcham, R. A. (2005a), Forward and inverse modelling of low-temperature thermochronology data, *Rev. Mineral. Geochem.*, *58*, 275–314, doi:10.2138/rmg.2005.58.11.

Ketcham, R. A. (2005b), The role of crystallographic angle in characterizing and modelling apatite fission-track length data, *Radiat. Meas.*, *39*, 595–601, doi:10.1016/j.radmeas.2004.07.008.

Ketcham, R. A., R. A. Donelick, and W. D. Carlson (1999), Variability of apatite fission-track annealing kinetics: III. Extrapolation to geological time scales, *Am. Mineral.*, *84*, 1235–1255.

Ketcham, R. A., A. Carter, R. A. Donelick, J. Barbarand, and A. J. Hurford (2007), Improved measurement of fission-track annealing in apatite using c-axis projection, *Am. Mineral.*, *92*, 789–798, doi:10.2138/am.2007.2280.

Knapp, J. H., C. C. Knapp, V. Raileanu, L. Matenco, V. Mocanu, and C. Dinu (2005), Crustal constraints on the origin of mantle seismicity in the Vrancea Zone, Romania: The case for active continental lithospheric delamination, *Tectonophysics*, *410*, 311–323, doi:10.1016/j.tecto.2005.02.020.

Kräutner, H. G. (1980), East Carpathians, in *Precambrian in Younger Fold Belts*, edited by V. Zoubek, pp. 625–638, Wiley, London.

Kräutner, H. G., and G. Bindea (2002), Structural units in the pre-Alpine basement of the Eastern Carpathians, *Geol. Carpathica*, *53*, 143–146.

Krézsek, C., and A. Bally (2006), The Transylvanian Basin (Romania) and its relation to the Carpathian fold and thrust belt: Insights in gravitational salt tectonics, *Mar. Pet. Geol.*, *23*, 405–442, doi:10.1016/j.marpetgeo.2006.03.003.

Krijgsman, W., F. J. Hilgen, I. Raffi, F. J. Sierro, and D. S. Wilson (1999), Chronology, causes and progression of the Messinian salinity crisis, *Nature*, *400*(6745), 652–655, doi:10.1038/23231.

Landes, M., W. Fielitz, F. Hauser, M. Popa, and C. Group (2004), 3-D upper-crustal tomographic structure across the Vrancea Seismic Zone, Romania, *Tectonophysics*, *382*, 85–102, doi:10.1016/j.tecto.2003.11.013.

Lăzărescu, V., and M. Popescu (1986), Shallow vs. deep, old vs. recent tectonic movements at the Eastern Carpathians arc bend, *Tectonophysics*, *131*, 287–299, doi:10.1016/0040-1951(86)90179-4.

Leever, K. (2007), Foreland of the Romanian Carpathians–controls on late orogenic sedimentary basin evolution and Paratethys paleogeography, Ph.D. thesis, 182 pp., Vrije Univ., Amsterdam.

Leever, K., L. Matenco, G. Bertotti, S. Cloetingh, and K. G. Drijkoningen (2006), Late orogenic vertical movements in the Carpathian bend zone–seismic constraints on the transition zone from orogen to foredeep, *Basin Res.*, *18*(4), 521–545, doi:10.1111/j.1365-2117.2006.00306.x.

Martin, M., et al. (2006), High-resolution teleseismic body wave tomography beneath SE-Romania–II. Imaging of a slab detachment scenario, *Geophys. J. Int.*, *164*, 579–595, doi:10.1111/j.1365-246X.2006.02884.x.

Matenco, L., and G. Bertotti (2000), Tertiary tectonic evolution of the external East Carpathians (Romania), *Tectonophysics*, *316*, 255–286, doi:10.1016/S0040-1951(99)00261-9.

Matenco, L., G. Bertotti, S. Cloetingh, and C. Dinu (2003), Subsidence analysis and tectonic evolution of the external Carpathian-Moesian Platform region during Neogene times, *Sediment. Geol.*, *156*, 71–94, doi:10.1016/S0037-0738(02)00283-X.

Matenco, L., G. Bertotti, K. Leever, S. Cloetingh, S. M. Schmid, M. Tărăpoancă, and C. Dinu (2007), Large-scale deformation in a locked collisional boundary: Interplay between subsidence and uplift, intraplate stress, and inherited lithospheric structure in the late stage of the SE Carpathians evolution, *Tectonics*, *26*, TC4011, doi:10.1029/2006TC001951.

Melinte, M. C., and D. Jipa (2005), Campanian-Maastrichtian marine red beds in Romania: Biostratigraphic and genetic significance, *Cretaceous Res.*, *26*(1), 49–56, doi:10.1016/j.cretres.2004.11.002.

Morley, C. K. (1996), Models for relative motion of crustal blocks within the Carpathian region, based on restorations of the outer Carpathian thrust sheets, *Tectonics*, *15*(4), 885–904, doi:10.1029/95TC03681.

Murgeanu, G. (1967), Geological map, scale 1:200,000, *Rep. 36*, Ploiesti, Com. de Stat al Geol., Inst. Geol., Bucharest.

Murrell, G. R. (2003), The long-term thermal evolution of central Fennoscandia revealed by low-temperature thermochronometry, Ph.D. thesis, 219 pp., Vrije Univ., Amsterdam.

Murrell, G. R., E. R. Sobel, B. Carrapa, and P. Andriessen (2009), Calibration and comparison of etching techniques for apatite fission-track thermochronology, in *Thermochronological Methods: From Palaeotemperature Constraints to Landscape Evolution Models*, edited by F. Lisker, B. Ventura, and U. Glasmacher, *Geol. Soc. Spec. Publ.*, *324*, 73–85, doi:10.1144/SP324.6.

Necea, D., W. Fielitz, and L. Matenco (2005), Late Pliocene–Quaternary tectonics in the frontal part of the SE Carpathians: Insights from tectonic geomorphology, *Tectonophysics*, *410*, 137–156, doi:10.1016/j.tecto.2005.05.047.

Oncescu, M.-C., and K.-P. Bonjer (1997), A note on the depth recurrence and strain release of large Vrancea earthquakes, *Tectonophysics*, *272*, 291–302, doi:10.1016/S0040-1951(96)00263-6.

Panaiotu, C. E., I. Vasiliev, C. G. Panaiotu, W. Krijgsman, and G. C. Langereis (2007), Provenance analysis as a key to orogenic exhumation: A case study from the East Carpathians (Romania), *Terra Nova*, *19*(2), 120–126, doi:10.1111/j.1365-3121.2006.00726.x.

Ratschbacher, L., H.-G. Linzer, F. Mozer, R.-O. Struziewicz, H. Bedelean, N. Han, and P.-A. Mogos (1993), Cretaceous to Miocene thrusting and wrenching along the Central South Carpathians due to a corner effect during collision and orocline formation, *Tectonics*, *12*(4), 855–873, doi:10.1029/93TC00232.

Rögl, F. (1996), Stratigraphic correlation of Paratethys Oligocene and Miocene, *Mitt. Ges. Geol. Bergbaustud. Österr.*, *41*, 65–73.

Royden, L. H., and B. C. Burchfiel (1989), Are systematic variations in thrust belt style related to plate boundary processes (the Western Alps versus the Carpathians), *Tectonics*, *8*, 51–61, doi:10.1029/TC008i001p00051.

Sacks, P. E., and D. T. Secor (1990), Delamination in collisional orogens, *Geology*, *18*, 999–1002, doi:10.1130/0091-7613(1990)018<0999:DICO>2.3.CO;2.

Sanders, C. A. E. (1998), Tectonics and erosion–Competitive forces in a compressive orogen: A

fission track study of the Romanian Carpathians, Ph.D. thesis, 204 pp., Vrije Univ., Amsterdam.

Sanders, C. A. E., P. A. M. Andriessen, and S. A. P. L. Cloetingh (1999), Life cycle of the East Carpathian orogen: Erosion history of a doubly vergent critical wedge assessed by fission-track thermochronology, *J. Geophys. Res.*, *104*(B12), 29,095–29,112, doi:10.1029/1998JB900046.

Săndulescu, M. (1984), *Geotectonica României*, 450 pp., Tehnicã, Bucharest.

Săndulescu, M. (1988), Cenozoic tectonic history of the Carpathians, in *The Pannonian Basin: A Study in Basin Evolution*, edited by L. H. Royden and F. Horváth, *AAPG Mem.*, *45*, 17–25.

Săndulescu, M. (1994), Overview on Romanian geology, *Rom. J. Tectonics Reg. Geol.*, *75*, suppl. 2, 3–15.

Săndulescu, M., M. Ştefănescu, A. Butac, I. Patrut, and P. Zaharescu (1981), *Genetical and Structural Relations Between Flysch and Molasse (The East Carpathians)*, 95 pp., Geol. Inst. of Rom., Bucharest.

Schmid, S. M., O. A. Pfiffner, N. Froitzheim, G. Schonborn, and E. Kissling (1996), Geophysical-geological transect and tectonic evolution of the Swiss-Italian Alps, *Tectonics*, *15*(5), 1036–1064, doi:10.1029/96TC00433.

Schmid, S. M., T. Berza, V. Diaconescu, N. Froitzheim, and B. Fügenschuh (1998), Orogen-parallel extension in the Southern Carpathians, *Tectonophysics*, *297*, 209–228, doi:10.1016/S0040-1951(98)00169-3.

Schmid, S. M., D. Bernoulli, B. Fügenschuh, L. Matenco, S. Schefer, R. Schuster, M. Tischler, and K. Ustaszewski (2008), The Alpine-Carpathian-Dinaridic orogenic system: Correlation and evolution of tectonic units, *Swiss J. Geosci.*, *101*(1), 139–183, doi:10.1007/s00015-008-1247-3.

Seghedi, I., H. Downes, A. Szakács, P. R. D. Mason, M. F. Thirlwall, E. Roşu, Z. Pécskay, E. Márton, and C. Panaiotu (2004), Neogene–Quaternary magmatism and geodynamics in the Carpathian–Pannonian region: A synthesis, *Lithos*, *72*, 117–146, doi:10.1016/j.lithos.2003.08.006.

Shuster, D. L., R. M. Flowers, and K. A. Farley (2006), The influence of natural radiation damage on helium diffusion kinetics in apatite, *Earth Planet. Sci. Lett.*, *249*(3–4), 148–161, doi:10.1016/j.epsl.2006.07.028.

Ştefănescu, M. (1976), A new image of the internal flysch structure From the Carpathian bend area, *Dari Seama Sedintelor Inst. Geol. Geofiz.*, *62*, 257–259.

Ştefănescu, M., and M. Mărunţeanu (1978), Age of the Doftana Molasse, *Dari de Seama ale Sedintelor Institutul de Geologie si Geofizica*, *65*, 169–182.

Ştefănescu, M., O. Dicea, and G. Tari (2000), Influence of extension and compression on salt diapirism in its type area, East Carpathians bend area, Romania, in *Salt, Shale and Igneous Diapirs in and Around Europe*, edited by B. C. Vendeville, Y. Mart, and J.-L. Vigneresse, *Geol. Soc. Spec. Publ.*, *174*, 131–147, doi:10.1144/GSL.SP.1999.174.01.08.

Stoica, M., I. Lazar, I. Vasiliev, and W. Krijgsman (2007), Mollusc assemblages of the Pontian and Dacian deposits from the Topolog-Argeş, area (southern Carpathian foredeep Romania), *Geobios*, *40*, 391–405, doi:10.1016/j.geobios.2006.11.004.

Tărăpoancă, M., G. Bertotti, L. Matenco, C. Dinu, and S. Cloetingh (2003), Architecture of the Focşani depression: A 13 km deep basin in the Carpathians bend zone (Romania), *Tectonics*, *22*(6), 1074, doi:10.1029/2002TC001486.

Ustaszewski, K., S. Schmid, B. Fügenschuh, M. Tischler, E. Kissling, and W. Spakman (2008), A map-view restoration of the Alpine-Carpathian-Dinaridic system for the Early Miocene, *Swiss J. Geosci.*, *101*, 273–294, doi:10.1007/s00015-008-1288-7.

Vasiliev, I. (2006), A new chronology for the Dacian Basin (Romania): Consequences for the kinematic and paleoenvironmental evolution of the Paratethys region, Ph.D. thesis, 193 pp., Univ. Utrecht, Utrecht, Netherlands.

Vasiliev, I., W. Krijgsman, C. G. Langereis, C. E. Panaiotu, L. Matenco, and G. Bertotti (2004), Towards an astrochronological framework for the eastern Paratethys Mio–Pliocene sedimentary sequences of the Focşani basin (Romania), *Earth Planet. Sci. Lett.*, *227*(1–2), 231–247, doi:10.1016/j.epsl.2004.09.012.

Veliciu, S., and M. Visarion (1984), Geothermal models for the East Carpathians, in *Terrestrial Heat Flow Studies and the Structure of the Lithosphere*, edited by V. Čermák, L. Rybach and D. S. Chapman, *Tectonophysics*, *103*, 157–165, doi:10.1016/0040-1951(84)90080-5.

Visarion, M., M. Săndulescu, D. Stănică, and L. Atanasiu (1988), An improved geotectonic model of the East Carpathians, *Rev. Roumania Geol. Geophys. Geogr. Ser. Geophys.*, *32*, 43–52.

Wagner, G. A., and P. van den Haute (1992), *Fission Track Dating*, 285 pp., Kluwer, Dordrecht, Netherlands.

Willett, S. D., and M. T. Brandon (2002), On steady states in mountain belts, *Geology*, *30*(2), 175–178, doi:10.1130/0091-7613(2002)030<0175:OSSIMB>2.0.CO;2.

Willett, S. D., F. Schlunegger, and V. Picotti (2006), Messinian climate change and erosional destruction of the central European Alps, *Geology*, *34*(8), 613–616, doi:10.1130/G22280.1.

Wortel, M. J. R., and W. Spakman (2000), Subduction and slab detachment in the Mediterranean-Carpathian Region, *Science*, *290*, 1910–1917, doi:10.1126/science.290.5498.1910.

Ziegler, P. A., S. Cloetingh, and J.-D. van Wees (1995), Dynamics of intra-plate compressional deformation: The Alpine foreland and other examples, *Tectonophysics*, *252*, 7–22, doi:10.1016/0040-1951(95)00102-6.

P. A. M. Andriessen, J. P. T. Foeken, and S. Merten, Department of Isotope Geochemistry, Faculty of Earth and Life Sciences, VU University, Amsterdam, NL-1081 HV, Netherlands. (sandra.merten@falw.vu.nl)

L. Matenco, Department of Tectonics, Faculty of Earth and Life Sciences, VU University, Amsterdam, NL-1081 HV, Netherlands.

F. M. Stuart, Isotope Geosciences Unit, Scottish Universities Environmental Research Centre, East Kilbride G75 0QF, UK.